Biomimetic microstimulation of sensory cortices

Christopher Hughes[1,2], Takashi Kozai[1-5,*]

1. Department of Bioengineering, University of Pittsburgh
2. Center for the Neural Basis of Cognition
3. Department of Neuroscience, University of Pittsburgh
4. McGowan Institute for Regenerative Medicine, University of Pittsburgh, Pittsburgh, PA, USA,
5. NeuroTech Center, University of Pittsburgh Brain Institute, Pittsburgh, PA, USA.

* corresponding author: tk.kozai@pitt.edu

Highlights

- Biomimetic amplitude modulation of intracortical microstimulation (ICMS) evokes distinct onset and offset transients in recruited neural populations
- Individual neurons can be separated into distinct classes based on their spatiotemporal responses to short (1 s) and long (30 s) as well as biomimetic or non-biomimetic ICMS profiles
- Adaptation to ICMS (decreases in evoked calcium intensity over time) are reduced for biomimetic amplitude trains
- Ideal observers (i.e. Bayesian classifiers) identify onset and offset of ICMS faster and more confidently with biomimetic amplitude modulation
- Biomimetic amplitude modulation of ICMS strongly signals onset and offset of stimulus input, reduces adaptation of neural activation, and decreases total charge injection for sensory feedback in brain-computer interfaces

Abstract

Background: Intracortical microstimulation (ICMS) is being researched to treat neurological disease or injury. Biomimetic microstimulation, or stimulus trains that mimic neural activity in the brain, made sensations more focal and natural in a human participant, but it is not understood how biomimetic microstimulation affects neural activation. Adaptation (decreases in evoked intensity over time) is also a potential barrier to clinical implementation of sensory feedback, and biomimetic microstimulation may reduce this effect.

Objective: We evaluated how biomimetic trains change the calcium response, spatial distribution, and adaptation of neurons in the somatosensory and visual cortices.

Methods: Calcium responses of neurons were measured in Layer 2/3 of visual and somatosensory cortices of anesthetized GCaMP6s mice in response to ICMS trains with fixed amplitude and frequency (Fixed) and three biomimetic ICMS trains that increased the stimulation intensity during the onset and offset of stimulation by modulating the amplitude (BioAmp), frequency (BioFreq), or amplitude and frequency (BioBoth). ICMS was provided for either 1-s with 4-s breaks (Short) or for 30-s with 15-s breaks (Long).

Results: BioAmp and BioBoth trains evoked distinct onset and offset transients in recruited neurons, while BioFreq trains evoked activity similar to Fixed trains. Biomimetic amplitude reduced adaptation (decreases in evoked calcium intensity) by 14.6±0.3% for Short and 36.1±0.6% for Long trains. Ideal observers were 0.031±0.009s faster for onset detection and 1.33±0.21s faster for offset detection with biomimetic amplitude.

Conclusions: Biomimetic amplitude modulation evokes distinct onset and offset transients, reduces adaptation, and decreases total charge injection for sensory feedback in brain-computer interfaces.

Introduction

Intracortical microstimulation (ICMS) has restored tactile sensation to the hands or arms of people with spinal cord injury [1]–[4] and restored vision in a person with blindness [5]. Tactile percepts range from natural sensations like “pressure” and “touch,” to less natural sensations like “tingle” and “buzz,” [1],[2] while visual percepts are dots or lines of light [5]. Animals discriminate ICMS and tactile frequencies similarly, so it was believed that ICMS evokes naturalistic sensations [9]–[11]. Humans also discriminate ICMS frequency, however,

percepts are often unnatural and electrode dependent [1],[8]. Additionally, percept adapt, or decrease in intensity over time, so that continuous stimulation can completely extinguish percepts within a minute [10], providing a clinical barrier for continuous restoration of sensation.

Normally, ICMS stimulus intensity is linearly matched to sensory input intensity, which improves robotic arm control [11]. Biomimetic ICMS that mimics cortical activity can potentially improve evoked percepts and efficacy [12]–[15]. In sensory cortices, neurons respond strongly to the onset and offset of sensory input with modest firing in between [16]–[18]. To mimic these strong transients, amplitude or frequency of ICMS can be elevated during onset and offset. Biomimetic algorithms use these principles [13],[19], which improved the naturalness and efficacy of peripheral nerve stimulation [20],[21]. Additionally, ICMS bio-inspired algorithms worked as well as linear algorithms with less charge injection for object identification [22] and reduced artifact in the motor cortex [23], which could be beneficial for bidirectional brain-computer interfaces [24]. Similar algorithms have reduced large onset transients for high-frequency stimulation in the hippocampus and nerve [25],[26].

Biomimetic ICMS improved the focality and naturalness of evoked sensations in preliminary results in a human [27], but it is not understood how biomimetic trains affect brain activation or adaptation [10],[28],[29]. Measuring the neural response to ICMS in humans is difficult due to safety and ethical concerns over human transgenic manipulation and limitations of hardware and high-resolution imaging. Transgenic mouse models with high-resolution imaging have been useful for studying how ICMS parameters affect the spatiotemporal response of the brain and how ICMS parameters can change neural responses [30]–[36].

Here we expand this work to understand how biomimetic ICMS trains affect neural activity relative to standard fixed-parameter ICMS trains using evoked calcium responses of neurons in Layer 2/3 of visual and somatosensory cortices of GCaMP6s mice. We found biomimetic amplitude modulation increases the activity at the onset and offset of ICMS and maintains excitability of neurons over long periods of stimulation while reducing the total charge injected.

Methods

Surgery and electrode implantation

Surgeries were performed on transgenic Thy1-GCaMP6s male (n=6) or female (n=6) mice (Jackson Laboratories, Bar Harbor, ME) >4 weeks of age weighing 25-35g. Anesthesia was induced with 75-mg/kg ketamine and 7-mg/kg xylazine administered intraperitoneally and updated with 45-mg/kg ketamine [12],[14]. Head-fixed mice were given rectangular craniotomies (2x3mm) over each visual cortex (n=8, long side 1mm from sagittal and short side <1mm from lambdoid suture) or somatosensory cortex (n=4, long side 1mm from coronal and short side 1mm from sagittal suture), with a dental drill (Fig. 1A). Cross-correlation (xcorr) was used to determine if the average evoked activity was similar across cortices, sex, and trial (Supp. Fig. 1-3). Single shank electrodes were 3mm long with 16 channels of 703µm^2 electrode sites spaced 50µm apart (NeuroNexus Technologies, Ann Arbor, MI) were implanted at a 30º angle using an oil-hydraulic Microdrive (MO-81, Narishige, Japan) to depths of 1000µm (Fig. 1B). Electrode sites were activated prior to experiments based on published protocols [37].

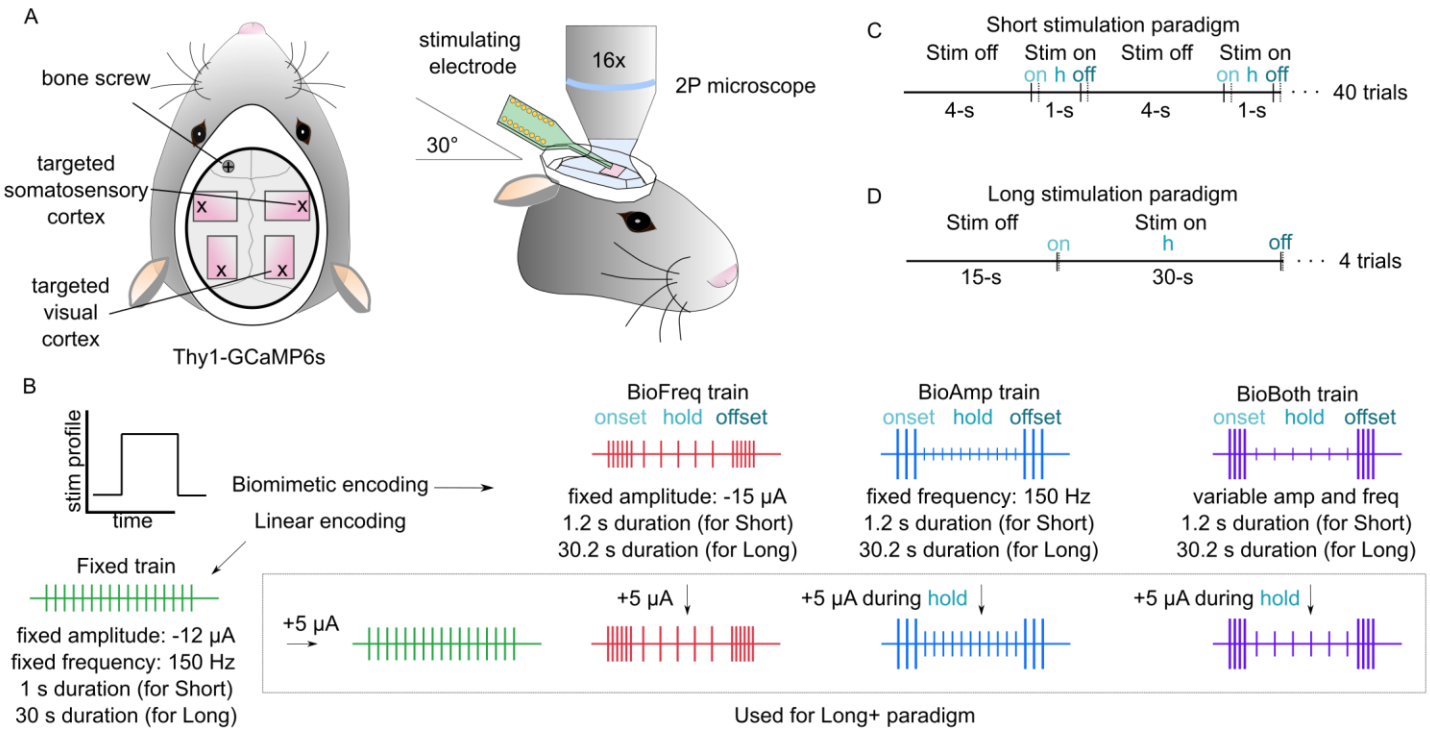

Figure 1: GCaMP6s mice received microstimulation through Michigan probes with simultaneous calcium imaging. A) We performed bilateral craniotomies in either the somatosensory or visual cortex. Electrodes were generally targeted to the right hemisphere unless there was bleeding or little activity evoked upon insertion. A bone screw was implanted in the left motor cortex for ground and reference. B) Two-photon imaging was used to image the open cranial window where ICMS was applied. Different ICMS trains were designed based on a transform from a fast ramp-and hold function to either directly entrain the sensory input (Fixed) or to emulate the response of sensory cortex that either varied the amplitude (BioAmp), frequency (BioFreq), or both (BioBoth) for a pulse train with onset, hold, and offset phases. All 1-s trains were designed to be charge matched. For the Long+ paradigm we increased the amplitude by 5 µA during the hold phase for BioAmp and BioBoth and during the whole train for BioFreq and Fixed (shown in the box) C) Short train paradigm. We delivered 1-s (or 1.2-s) pulse trains followed by 4-s (or 3.8-s) breaks for 40 trials per block. Onset, hold, and offset phases are marked with "on," "h", and "off" and indicated by the vertical lines D) Long train paradigm. We delivered 30-s (or 30.2-s) pulse trains with 15-s (or 14.8-s) breaks for 4 trials per block.

Electrical stimulation

A TDT IZ2 stimulator controlled by an RZ5D system (Tucker-Davis Technologies, Alachua, FL) applied current-controlled cathodic leading biphasic asymmetric pulses (200-µs cathodic, 100-µs interphase, 400-µs anodic), which matched human experiments [1],[5]. Amplitudes in the range of 0-20µA and frequencies of 0-200Hz were used based on safety limits to reduce electrode/tissue damage [21],[22]. Only one electrode localized to the imaging plane (120-200µm below the surface) with an impedance <700 kOhms was used in each animal.

Biomimetic stimulation parameters

Fixed-parameter trains delivered a constant amplitude and frequency (Fixed). Biomimetic trains provided high-intensity "onset" and "offset" transients (200-ms in length) with high amplitude (BioAmp), frequency (BioFreq), or both (BioBoth) (Figure 1A, Table 1) with a 25% low-intensity "hold" phase in between (Fig. 1B). The 200-ms offset phase for each biomimetic train signaled the end of stimulus input which resulted in an additional 200ms of ICMS compared to the Fixed train. For Short trains, each animal was stimulated for 1-s (or 1.2-s) of ICMS followed by 4-s (or 3.8-s) of rest for 40 trials. For Long trains, each mouse was stimulated for 30-s (or 30.2-s) of ICMS followed by 15-s (or 14.8-s) of rest for 4 trials. Train order was randomized to remove ordering effects. All Short trains were symmetric and had equal total charge injection (360nC, Table 1). For Long trains, a consistent transient "onset" and "offset" period (200-ms) was applied but with an extended "hold" phase (28.8-s), which resulted in unequal charge injection across trains, with lowest charge injection for BioBoth (1760nC) and highest charge injection for Fixed trains (10800nC). A version of each Long train where the amplitude of the whole train (for BioFreq and Fixed) or the hold phase (for BioAmp and BioBoth) was increased by 5µA to measure how increases in amplitude changed activity (Long+ trains). Data from 12 mice are presented here (Supp. Table 1).

		Onset			Hold			Offset			
		Amp (µA)	**Freq (Hz)**	**Dur (s)**	**Amp (µA)**	**Freq (Hz)**	**Dur (s)**	**Amp (µA)**	**Freq (Hz)**	**Dur (s)**	**Total charge (cathodic phase for all pulses, nC)**
BioAmp	**Short**	-20	150	0.2	-5	150	0.8	-20	150	0.2	360
	Long	-20	150	0.2	-5	150	28.8	-20	150	0.2	4560
	Long+	-20	150	0.2	-10	150	28.8	-20	150	0.2	8880
BioFreq	**Short**	-15	200	0.2	-15	50	0.8	-15	200	0.2	360
	Long	-15	200	0.2	-15	50	28.8	-15	200	0.2	4560
	Long+	-20	200	0.2	-20	50	28.8	-20	200	0.2	6080
BioBoth	**Short**	-20	200	0.2	-5	50	0.8	-20	200	0.2	360
	Long	-20	200	0.2	-5	50	28.8	-20	200	0.2	1760
	Long+	-20	200	0.2	-5	50	28.8	-20	200	0.2	3200
Fixed	**Short**	X	X	X	-12	150	1	X	X	X	360
	Long	X	X	X	-12	150	30	X	X	X	10800
	Long+	X	X	X	-17	150	30	X	X	X	15300

Table 1: **Outline of the parameters used in each ICMS train and paradigm.** While amplitude, frequency, and duration differed across trains, the overall charge injected was equivalent for the Short trains, but different for the Long and Long+ trains. The Fixed trains did not have distinct onset and offset phases, so all parameters are included in the hold phase.

Two-photon imaging

A two-photon laser scanning microscope (Bruker, Madison, WI) with a 16X 0.8 numerical aperture water immersion objective lens (Nikon Instruments, Melville, NY) and an OPO laser (Insight DS+; Spectra-Physics, Menlo Park, CA) tuned to a wavelength of 920nm were used. Time series images were recorded at 30Hz and 1.52× optical zoom with 512x512 pixel resolution with a total coverage of 543.2x543.2µm.

Image processing

Cells were manually outlined using 2D projections of the standard deviation and grouped averages of fluorescence using ImageJ (NIH). In animals with no significant shifts in the imaging plane across trials, a consistent region-of-interest (ROI) map was used to make comparisons of individual ROIs across trains. The mean fluorescence of each ROI was extracted over time and imported to MATLAB (Mathworks, Natick, MA). All fluorescence data was filtered using a 15-sample Gaussian temporal filter to remove noise artifact. Fluorescent intensity was normalized to the baseline (dF/F0) at the beginning of the trial (3-s for Short, 14-s for Long). ROIs were parsed into active and inactive populations with a threshold of +3 standard deviations of baseline. For Short trains, onset was 0 to 1s after ICMS start and offset was from 1 to 2s. For Long trains, onset was 0 to 3s after ICMS start, hold was from 3 to 30s, and offset was from 30 to 33s. For illustration, images shown were smoothed using singular value decomposition, but were not smoothed for analyses.

Labeling of individual neurons responses

Neurons were divided into groups based on temporal characteristics of the calcium evoked responses (Supp. Fig. 4). “Modulated” ROIs had onset and offset activity greater than the maximum of the hold phase by ½ standard deviations (SDs). “Onset” ROIs had onset peaks that had a larger maximum than the offset peaks by at least ½ SDs, while this relationship was reversed for the “Offset” ROIs and activity was not different for the “Same” ROIs. “Rapidly Adapting (RA)” ROIs had a maximum activation at the beginning of the hold period that was less than half of the maximum activation during the onset. “Slowly Adapting” (SA) ROIs had a maximum activation in the first half of the hold phase that was greater than the maximum in the second half by at least ½ SDs. “Steady State” (SS) ROIs had no difference across the hold phase within ½ SD.

To determine if the response of an individual ROI to one pulse train was predictive of its response to other trains, labels were grouped across trains within single ROIs and a correlation index (*CI*) was calculated with:

$$CI_{L2|L1} = \frac{L2|L1}{\%L2 * \#L1} \qquad \text{[Eq.1]}$$

where *L2*|*L1* is the amount of times label 2 (*L2*) occurred for one train (train 2) given the occurrence of label 1 (*L1*) for a different train (train 1), *%L2* represents the % of labels for train 2 made up by *L2*, and *#L1* is the total occurrences of *L1* for train 1. The *CI* converges to 1 if the labels occurred by chance and is greater or less than 1 if the correlation is greater or less than chance, respectively. Labels were randomly sorted for active ROIs 10,000 times and the *CI* was calculated each time to produce a distribution of *CI*s that occurred by chance. A pseudo p-value was calculated by comparing the real *CI* to the random distribution (Supp. Fig. 5).

Adaptation indices

Adaptation indices (*AI*s) of fluorescent intensity for continuous ICMS were calculated with:

$$AI = \frac{abs(A) - abs(B)}{abs(A) + abs(B)} \quad \text{[Eq.2]}$$

where *A* represents the mean activity in an ROI during the first half of the evoked response and *B* represents the mean activity in the second half of the evoked response. For cross-trial adaptation, the mean was calculated across all active ROIs within a trial and *A* is the first trial while *B* is the last trial. An *AI* of 1 would demonstrate maximal adaptation, 0 no adaptation, and -1 maximal facilitation (increase in activity).

Ideal observer analysis

An ideal observer classifies stimuli (based on evoked responses) in a statistically optimal manner determined by the arguments of maxima from Baye's formula (i.e. Bayesian classification) [40]. Ideal observer analysis has been used previously to classify sensory and ICMS evoked responses with voltage-sensitive dyes [41],[42]. Here, Bayesian classifiers were trained on the average fluorescent activity across ROIs in response to Long trains.

Onset and offset detection were determined with two encoding models: a biomimetic and fixed model (Supp. Fig. 6A). The biomimetic model identified "onset" and "offset" based on high intensity transients. The fixed model identified "on" or "off" based on elevated intensity. The states of the stimulus ("onset/offset", "on", "off") were labeled where the calcium activity was greater than 0.5x SDs baseline. Bayesian classifiers, which leverage Baye's theorem to assign observations the most probable class based on the maximum posterior probability [43], were trained using the "fitcnb" function in MATLAB and classification scores were returned using the "resubPredict" function. Each train was trained with both models and the best encoding model for each train was determined from the area under the curve for the receiver-operating characteristic (Supp. Fig. 6B). The inputs were dF/F_0 profiles and corresponding labels of the stimulus state. Onset and offset detection times (DTs) were the times classifier scores reached 75% confidence in the predicted class labels. A false positive was when 75% confidence was achieved before the known onset or offset, and trials with false positives were excluded from calculation of average onset and offset times. A simpler thresholding method was also applied, in which changes in state were determined with a threshold of +3 SDs baseline (Supp. Fig. 6C,D).

For discrimination of stimulus intensity, activity during the hold phase was adjusted with Eq. 3 (to account for adaptation) and each classifier was trained to distinguish low amplitude trains from paired high amplitude trains. Accuracy of the classifiers were summed across animals and significant differences were calculated between accuracies for each train.

Statistics

All statistical analysis were conducted in MATLAB. All data were compared for significant differences at an α of 0.05 using ANOVA followed by Tukey's HSD to identify pairwise differences and account for multiple comparisons unless otherwise noted. Significance is indicated in figures with * for $p<0.05$, ** for $p<0.01$, and *** for $p<0.001$. Violin plots were generated by estimating the kernel density using ksdensity() and cutting off values at min/max possible values [44]. All means are reported ±SE.

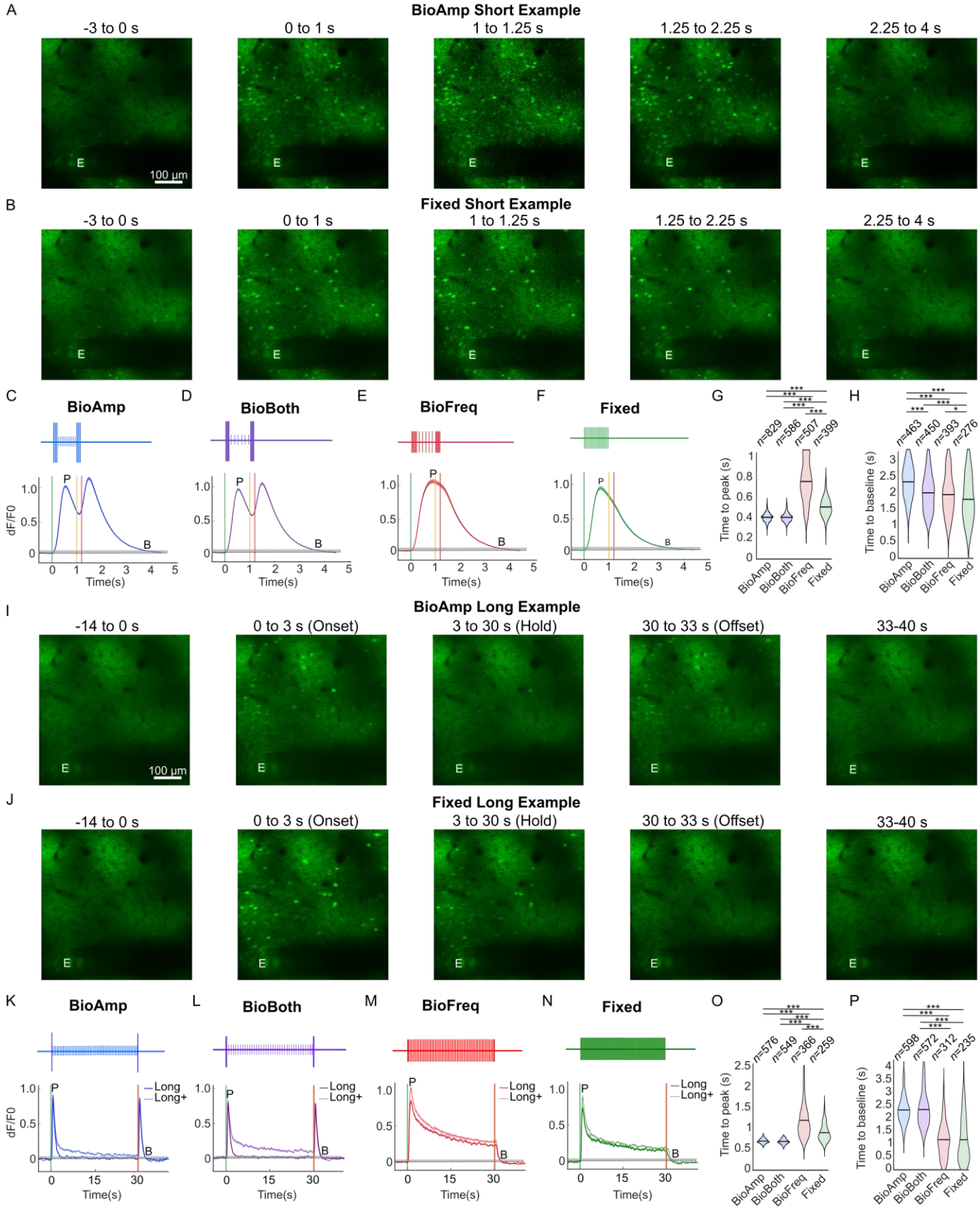

Figure 2: Biomimetic amplitude modulated trains evoke strong onset and offset transients, while biomimetic frequency or fixed trains evoke general increases that adapt over time. A-B) Examples of 2P images of evoked activity for a Short BioAmp (A) and Fixed (B) train. The "E" marks the stimulated electrode location. Scale bar=100 µm wide, 10 µm thick. C-H) Short trains (*n*=12 animals) C-D) BioAmp and BioBoth trains evoked increases in the intensity during the onset and offset phases. Each trace shows the average activity across all ROIs and the shaded region shows the standard error. Vertical dotted lines mark the onset start (green), offset start (yellow), and offset end (red). The grey box represents 0.5x the standard deviation of the average baseline across all ROIs. The letters "P" and "B" mark the location of the time-to-peak and time-to-baseline for the average trace. E-F) BioFreq and Fixed trains evoked similar profiles. G) BioAmp and BioBoth trains achieved a faster time to peak than the BioFreq and Fixed trains. The size of the violin represents the kernel density estimate of the sample, the black bar shows the mean. Outliers more than three scaled median absolute deviations

from the median were excluded for illustration. H) Fixed trains returned to baseline faster than the other trains. I-J) Examples of 2P images for Long BioAmp (I) and Fixed (J) trains. K-P) Long (solid lines, *n*=9 animals) and Long+ (dotted lines, *n*=7 animals) trains. K-L) BioAmp and BioBoth trains reduced activation during the hold phase, maintaining excitability for the offset transient. M-N) BioFreq and Fixed trains maintained strong activation during the hold phase driving adaptation. O-P) BioAmp and BioBoth trains achieved peak faster and baseline slower than Fixed and BioFreq trains.

Results

Biomimetic amplitude, but not frequency, modulation evokes distinct onset and offset transients in recruited neurons

The average neural activity evoked was similar across visual and somatosensory cortices, animal sex, and trials (xcorr vis vs. som=0.998, Supp. Fig. 1, xcorr male vs. female=0.998, Supp. Fig. 2, xcorr trial1 vs trial2=0.995, Supp. Fig. 3). Short ICMS trains evoked calcium activity for 3.04±0.009s following onset (Fig. 2A,B). Biomimetic amplitude modulation resulted in distinct onset and offset transients (Fig. 2C,D), but biomimetic frequency modulation alone (Fig. 2E) did not and the response closely resembled the response to Fixed trains (Fig. 2D). Biomimetic amplitude Short trains resulted in faster times-to-peak (BioAmp=0.40±0.001s, BioBoth=0.40±0.002s vs. BioFreq=0.75±0.009s, Fixed=0.50±0.004s) and slower recovery to baseline (BioAmp=2.31±0.024s, BioBoth=1.97±0.027s vs. BioFreq=1.91±0.032s and Fixed=1.77±0.043s, Fig. 2G,H). Long and Long+ trains evoked similar responses to Short trains but with extended hold phases. Biomimetic amplitude trains weakly activated neurons during the hold phase which maintained excitability for the offset, while BioFreq and Fixed trains adapted over time (Fig. 2I-N). Average evoked activity recovered to baseline in less than 2.5s for all trains.

For Short trains (1-s on, 4-s off), BioAmp elicited activity in the most ROIs (active ROIs=58±9%, p=0.15, Fig. 3B) with the highest intensity (mean dF/F0=1.12±0.022 from 0 to 2.5s, p<0.001, Fig. 3C) and BioBoth elicited activity farthest from the electrode (mean distance=200±6.2µm, p<0.05, Fig. 3D). For Long trains (30-s on, 15-s off), BioAmp and BioBoth elicited activity in the most ROIs during onset (58±10% and 55±9%) although the difference was not significant (p=0.12, Fig. 3E). The BioFreq and Fixed trains elicited a stronger mean intensity during onset (dF/F0=0.60±0.022 and 0.49±0.028), because BioAmp and BioBoth (dF/F0=0.31±0.01 and 0.28±0.01) decreased towards baseline in this defined interval (Fig. 3F). During the hold phase, BioAmp and BioBoth trains evoked much lower activity overall (active ROIs=2.9±0.9% and 3.9±1.5%, mean dF/F0=0.27±0.06 and 0.27±0.05) than BioFreq and Fixed (active ROIs=34±7.3% and 17±3.9%, mean dF/F0=0.33±0.02 and 0.36±0.02) as expected due to the 75% reduction in amplitude (p<0.001, Fig. 3E,F). For offset, BioAmp and BioBoth trains evoked activity in more ROIs (active ROIs=58±10% and 51±9%) at higher intensities (mean dF/F0=0.35±0.01 and 0.35±0.01) than BioFreq and Fixed (active ROIs=12±3.5% and 4.6±1.2%, mean dF/F0=0.19±0.01 and 0.23±0.02, p<0.001, Fig. 3E,F). BioAmp trains elicited activity in neurons farthest from the electrode in all phases (Fig. 3G). Long+ trains evoked similar responses to Long trains (Fig. 3H-J). Overall, biomimetic amplitude modulation increased the activation during onset and offset and activated neurons farther from the electrode.

Individual neuron responses divide into distinct spatiotemporal classes

Individual neurons had distinct responses, which were dependent on the train type and the length of stimulation. Most active ROIs had similar responses to Short trains (Fig. 4A-D). BioAmp and BioBoth ROIs were divided into three categories: higher intensity at onset (Onset), offset (Offset), or no difference (Same, Fig. 4A-B). While most ROIs responded similarly to BioFreq and Fixed trains, a subgroup were modulated by dynamic changes in frequency for BioFreq (Modulated, 5%, Fig. 4C).

For Long and Long+ trains, BioAmp and BioBoth divided similarly into Onset, Offset, or Same (Fig. 4E,F). The Long+ trains evoked more Onset responses, likely because the higher amplitude adapted neurons, resulting in a decrease in the second peak intensity (avg. decrease peak-to-peak: BioAmp=14±1.0%, BioBoth=16±1.0%). However, some ROIs had elevated activity during the hold phase in response to BioAmp and BioBoth trains especially for Long+. These ROIs were divided into two categories: slowly adapting (SA) activity over time or consistent elevation (Steady State, SS). SA ROIs decreased in intensity for the offset peak relative to the onset peak (avg. decrease peak-to-peak, Long: BioAmp=0.5±7.9%, BioBoth=12.5±7.8%, Long+: BioAmp=27±3.5%, BioBoth=39±2.4%), demonstrating a decrease in excitability of the neuron (Fig. 4E,F). SS neurons showed an increase in the second peak for Long trains (avg. increase peak-to-peak: BioAmp=19±6.3%, BioBoth=31±14%) demonstrating an increase in the excitability of the neuron, but showed a small decrease for Long+ (avg. decrease peak-to-peak: BioAmp=6±3.8%, BioBoth=16±5.8%).

BioFreq and Fixed ROIs were classified similarly into SA and SS, as well as rapid adapting (RA) (Fig. 4G,H). Fixed trains evoked more RA responses (Long=52%, Long+=58%) than BioFreq (Long=23%, Long+=25%), likely because the higher frequency during the hold phase adapted neurons more strongly. Long+ trains also evoked more RA responses (Long+: BioFreq=25%, Fixed=58% vs. Long: BioFreq=23%, Fixed=52%) and less SS responses (Long+: BioFreq=12%, Fixed=12% vs. Long: BioFreq=20%, Fixed=21%) than Long, likely because the higher amplitude adapted neurons more strongly. Similar to Short trains, a subpopulation were modulated by dynamic changes in frequency (Modulated, 1%) which were significantly farther from the electrode for Long trains (p<0.01, mean distance=441µm).

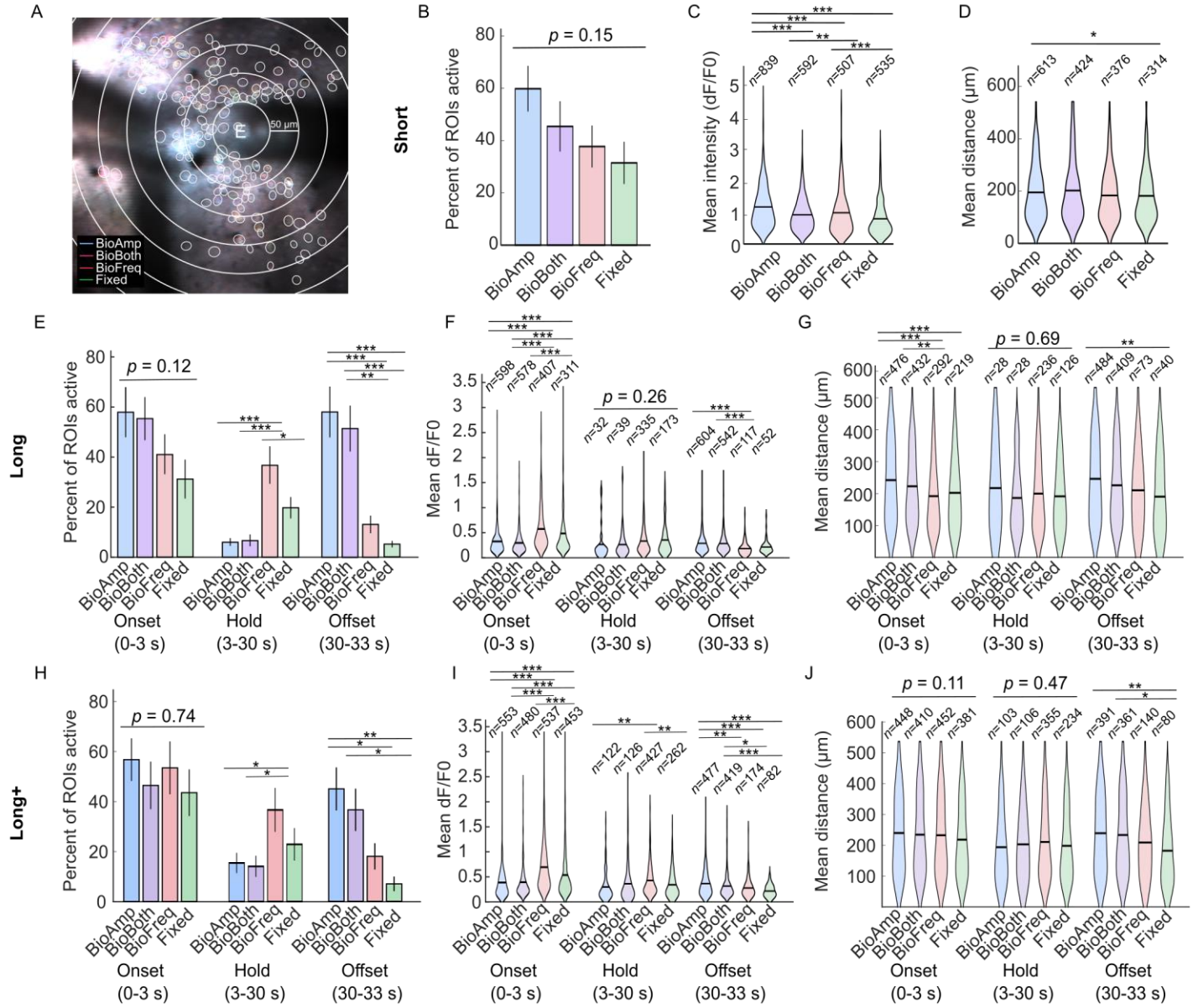

Figure 3: Biomimetic amplitude modulated trains evoke activity in more neurons during the onset and offset phase and recruit neurons farther from the electrode. A) Example of an evoked response to Short stimulation for BioAmp, BioBoth, BioFreq, and Fixed trains. The evoked response to each train type was set to a different color as indicated in the legend, and all colors were merged into a single image. The electrode location is marked with "E." Circles were drawn with radii of 50 µm away from the electrode to illustrate the distance of ROIs from the electrode. ROIs labeled across all trains are indicated with white ellipses, based on exported manual labels from ImageJ that were fit with an ellipse in MATLAB [45]. B-D) Biomimetic amplitude modulation increases the percent of active ROIs for Short trains (n=12 animals) (B), mean fluorescence evoked from stimulation start to 2.5 s after stimulation onset (C), and mean distance from the electrode (D) for active ROIs during the Short paradigm. The bars for % active show the mean while the error bars show the standard error. The size of the violin represents the kernel density estimate of the sample, the black bar shows the mean. E-J) Biomimetic amplitude modulation increases activity during the onset and offset phases, but decreases activation during the hold phase, while generally activating neurons farther from the electrode. E) The percent of active ROIs (n=9 animals), F) the mean fluorescence, and G) the mean distance from the electrode (F) for active ROIs during the Long paradigm. H-J) The total percent of active ROIs (n=7 animals) (H), mean fluorescence (I), and mean distance from the electrode (J) for active ROIs during the Long+ paradigm.

Across all trains, SS ROIs were closest to the electrode, while RA neurons were farthest (Fig. 4E-L). Labels for ROIs were consistent between Short BioAmp and BioBoth trains as well as Long and Long+ BioFreq and Fixed trains (p<0.05, Eq. 1), but labels in BioAmp and BioBoth were never predictive of labels for BioFreq and Fixed, and labels for Short were never predictive of labels for Long or Long+ (p>0.05, Supp. Fig. 5). Overall, BioAmp and BioBoth trains evoked similar responses while BioFreq and Fixed evoked similar responses. Long and Long+ trains were distinguished from Short trains by the different types of adaptation that occurred across neurons.

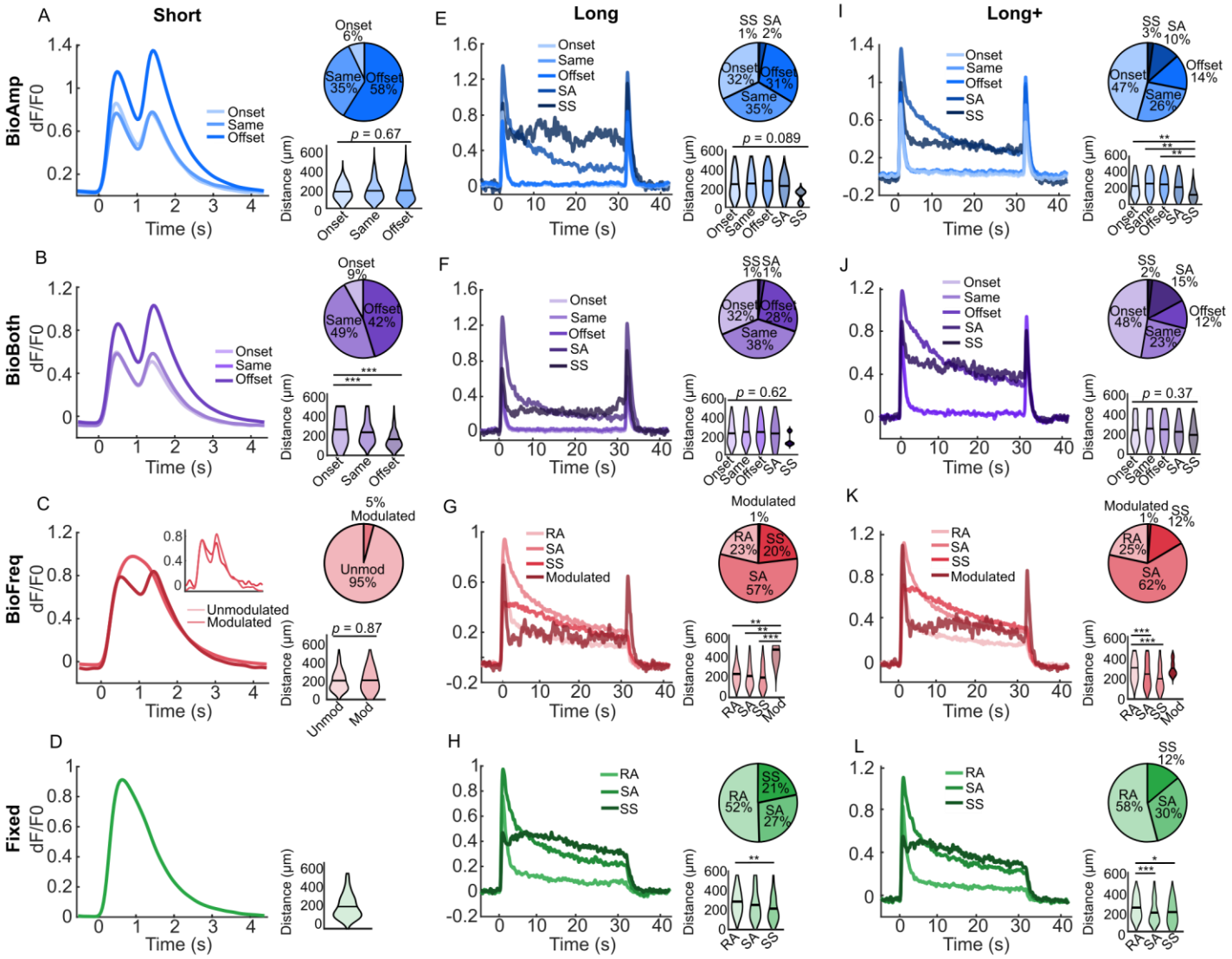

Figure 4: Individual neurons can be separated into distinct classes based on their unique spatiotemporal responses to each ICMS train. Each panel shows the corresponding average traces for each class, the total percent of ROIs in each class (pie plot), and the distance of the ROIs of each class from the electrode (violin plot of active ROIs). A-D) Response to Short trains. A-B) Individual ROIs have the greatest intensity either at the onset phase, offset phase, or had the same intensities at both peaks for BioAmp (A) and BioBoth (B) trains. C) Individual ROIs respond very consistently except a small subpopulation that are responsive to the onset and offset of ICMS (Modulated) for BioFreq trains. D) Fixed trains could not be reasonably divided into more than one category. E-H) Response to Long trains. E-F) Individual ROIs respond similarly to the short trains for BioAmp (E) and BioBoth (F) trains, but also contain some ROIs with elevated activity during the hold, which are divided into slowly adapting (SA) and steady state (SS) type responses. G-H) Individual ROIs can be divided into those that show rapid adaptation in the first 10-s of ICMS (RA), those that have slow adaptation throughout the 30-s of ICMS (SA), or those that have sustained activity throughout (Steady State, SS) for the BioFreq (G) and Fixed (H) trains. I-L) Response to Long+ trains. I-J) Individual ROIs respond similarly to the Long trains except with more ROIs active during the hold phase for the BioAmp (I) and BioBoth (J) trains. K-L) Individual ROIs were divided into identical classes as the Long trains for BioFreq (K) and Fixed (L) trains.

Adaptation of evoked activity is reduced with biomimetic amplitude modulation

For continuous stimulation, BioAmp and BioBoth Short trains drove minor facilitation (mean adaptation-index (AI)=-0.04±0.002 and -0.03±0.003, respectively, Eq. 2), while BioFreq and Fixed drove adaptation (AI=0.05±0.003 and 0.18±0.006, p<0.001, Fig. 5B). BioAmp and BioBoth Long trains drove minor adaptation

(*AI*=0.009±0.004 and 0.012±0.004) while BioFreq and Fixed drove stronger adaptation (*AI*=0.37±0.009 and 0.35±0.013, *p*<0.001, Fig 5C). Long+ trains increased adaptation for all trains, but BioAmp and BioBoth (*AI*=0.09±0.006 and 0.1±0.006) still drove less adaptation than BioFreq and Fixed (*AI*=0.37±0.008 and 0.43±0.01, *p*<0.001, Fig. 5D).

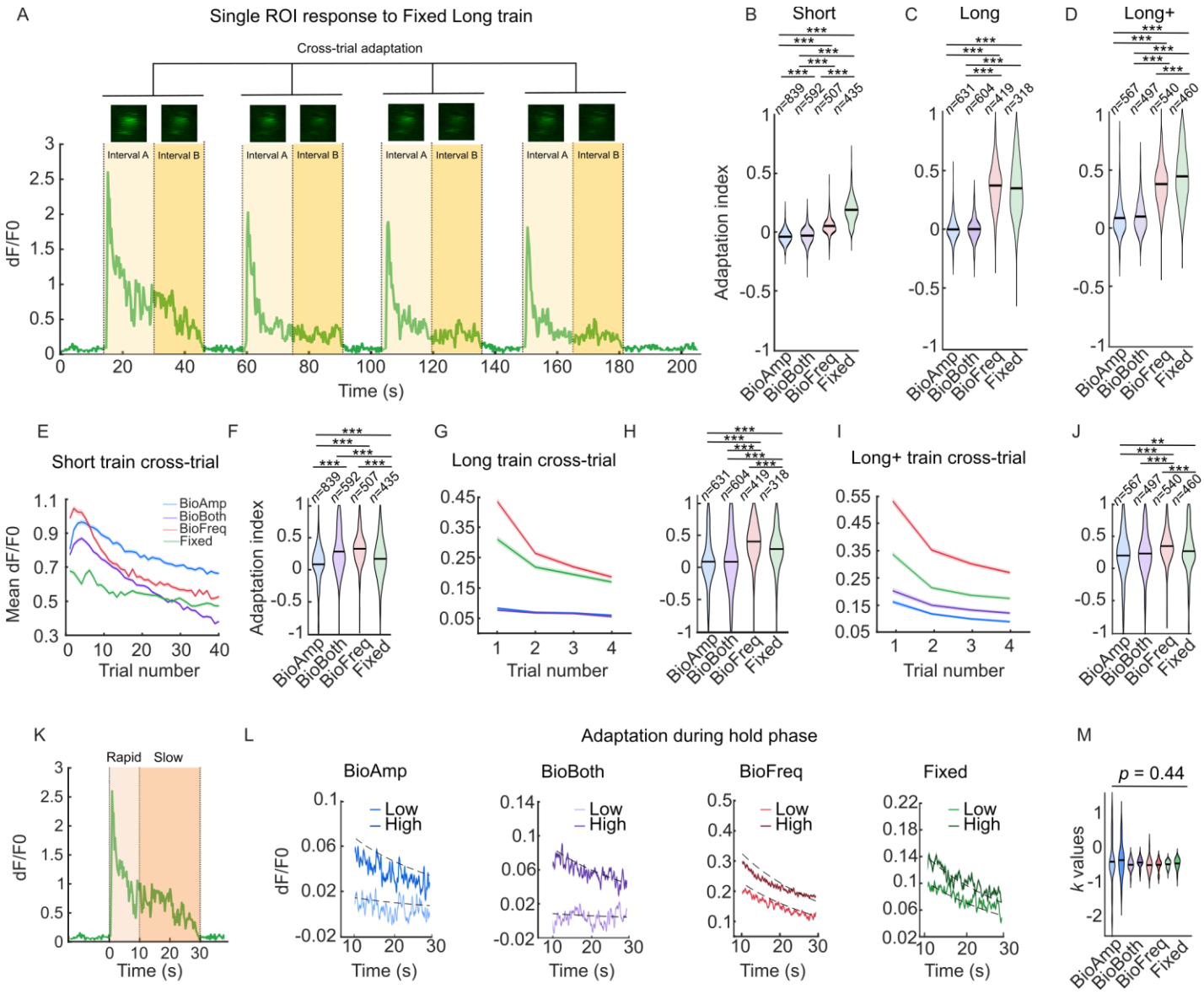

Figure 5: Adaptation occurs less for biomimetic amplitude stimulation than biomimetic frequency or fixed parameter stimulation. A) An example of a single ROI showing adaptation to a Fixed Long train. Adaptation indices for continuous stimulation were calculated using Intervals A and B with Equation 2. Cross-trial adaptation was calculated using the average intensity from each trial and using the first and last trial. B-D) Adaptation indices (when comparing the first half to the second half of the train) were greater for the BioFreq and Fixed trains than the BioAmp and BioBoth trains for the Short (B), Long (C), and Long+ (D) paradigms., indicating stronger adaptation E-J) Biomimetic amplitude modulation generally decreases adaptation across trials for Short trains (E-F), Long trains (G-H), and Long+ trains (I-J). E,G,I) The mean dF/F0 of all active ROIs is plotted across trials and the standard error is marked by the shaded region. F,H,J) Adaptation indices for all active ROIs are shown by the violin plot. K) The same trace from (A) is used to demonstrate the division of the Long and Long+ trials into the "rapid" and "slow" adaptation phases. L) Adaptation during the slow phase occurs consistently as a function of the starting intensity across trains. Average intensity traces for each Long and Long+ train are plotted for the hold phase. Adaptation during this period can be accounted for with Equation 2, which is shown by the dotted line. M) Violin plots showing the adaptation slopes for each train during the slow phase (*n*=21-26). Note that none of these slopes are significantly different.

Adaptation was also assessed across trials. Short trains drove facilitation across the first three trials, followed by adaptation (Fig. 5E). BioAmp trains drove the least adaptation (*AI*=0.09±0.01) and BioFreq drove the most (*AI*=0.33±0.01, *p*<0.001, Fig. 5F). For Long trains, no facilitation occurred and the strongest adaptation occurred from the first to the second trial (Fig. 5G). BioAmp and BioBoth trains drove less adaptation across trials (*AI*=0.1±0.015 and 0.1±0.018) than BioFreq and Fixed (*AI*=0.41±0.014 and 0.29±0.017, *p*<0.001, Fig. 5H). For

Long+ trains, BioFreq had the highest adaptation (*AI*=0.34±0.01) while BioAmp had the least (*AI*=0.21±0.016, *p*<0.001, Fig. 5I,J).

Adaptation was divided into two phases for Long trains, an initial rapid adaptation (the first 10s) and a slower adaptation (the last 20s) (Fig. 5K). While rapid adaptation was dependent on the parameters of ICMS delivered, slow adaptation was consistent for the parameters used here, and could be described with a simple equation using only the starting intensity:

$$I(t) = k * I_0 * \ln(t) + I_0 \qquad \text{[Eq.3]}$$

where I(t) is the intensity at time point t, ln(t) is the natural log of the time axis (with range 10-30s), I_0 is the intensity at the start of the hold phase, and *k* is a constant where $k*I_0$ describes the slope. For all Long and Long+ trains, *k* = -0.43±0.04 was used to fit average traces (Fig. 5L) and it was found that *k* values were not significantly different between trains (*p*=0.44, Fig. 5M) indicating consistency in slow adaptation for all parameters used here. Overall, biomimetic amplitude modulation reduced adaptation within and across trials, although adaptation during the slow adaptation phase (20-30s) seemed to be independent of stimulus parameters and only dependent on the starting intensity.

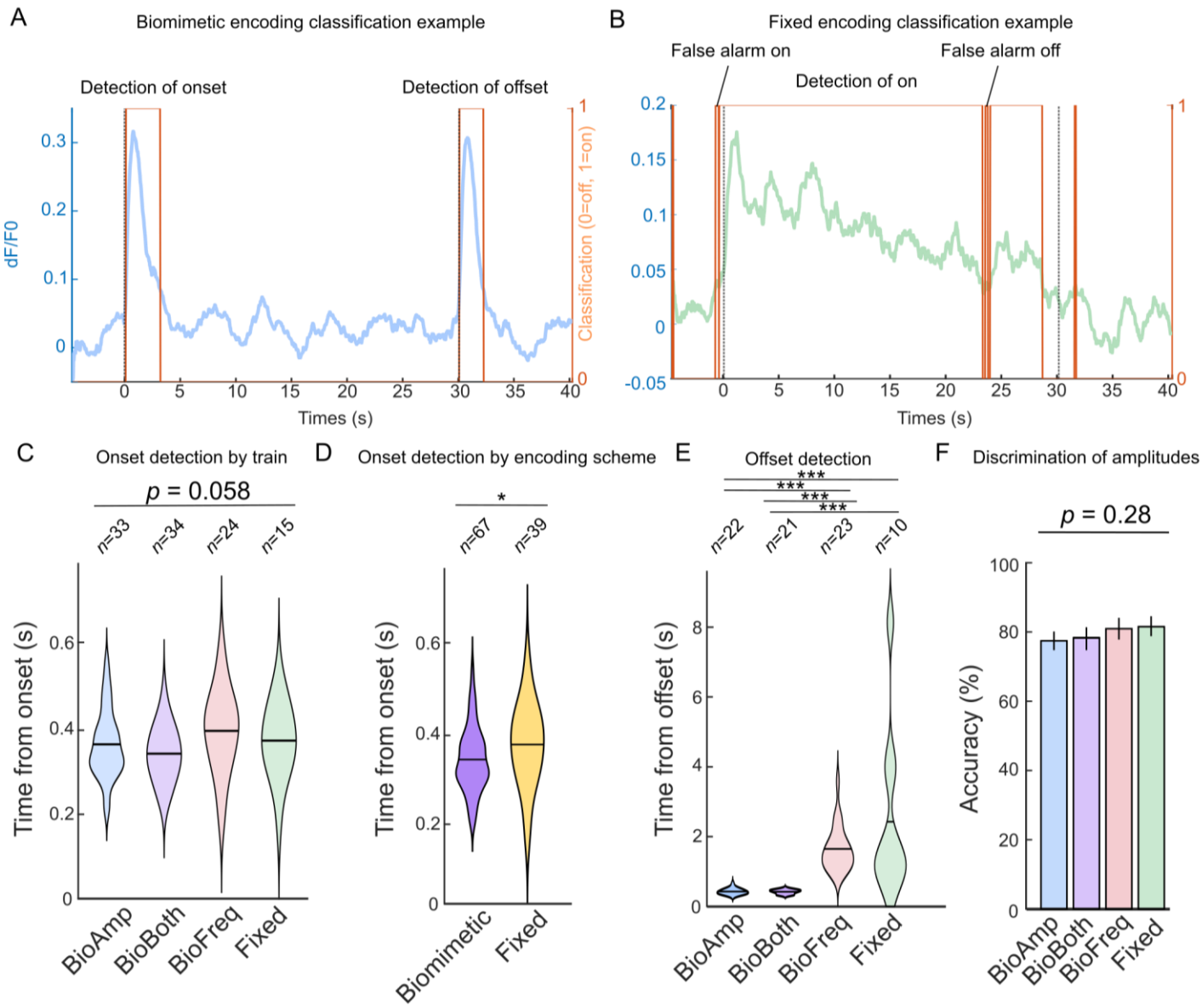

Figure 6: Bayesian classification of ICMS evoked profiles demonstrates improved identification of onset and offset for biomimetic amplitude modulated trains. A) Example of classification of a Long BioAmp train response using the biomimetic encoding model. The blue trace shows the fluorescent intensity evoked by ICMS and the orange trace shows the classification of the onset and offset state (based on confidence>75%). The black dotted line indicates the real stimulation onset and offset. B) Example of classification of a Long Fixed train response using the fixed encoding model, with examples of false alarms for stim on and stim off. A false alarm was defined as confidence of on>75% before stimulation onset or confidence in off>75% before stimulus offset. C-D) Biomimetic encoding with the amplitude modulated trains improved onset detection slightly. C) Violin plot of time to onset detection for each train type. Time to onset was calculated as the time point in which 75% confidence was achieved in onset. Trials on which onset was determined before stimulus onset were considered false alarms and excluded from analysis. The size of the violin represents the kernel density estimate of the *n* trials, the black bar shows the mean. D) Time to onset detection for each encoding scheme. Results from the BioAmp and BioBoth trains were for the biomimetic encoding model while results from the BioFreq and Fixed trains were combined for the Fixed model. E) Biomimetic encoding greatly reduced the time to offset detection. F) All trains resulted in high accuracy (>75%) at discriminating high amplitude from low amplitudes. Accuracy for amplitude discrimination for each train type across all trains (*n*=28 trials). Total accuracy was based on the correct identification of each time point as being the lower or higher amplitude train. Error bars show standard error.

Ideal observers classify stimulus onset and offset faster with biomimetic amplitude modulation

Higher amplitudes of ICMS can result in better detection of stimulus input [4],[8],[46]–[48]. Therefore, high amplitude transients that signal stimulus onset and offset might lead to faster detection of stimulus onset and offset. Ideal observer analysis (IDA i.e. Bayesian classification) was used to quantify the information about sensory input contained in the calcium activity evoked by each train. Two encoding schemes were used: biomimetic (detection of onset and offset transients) and linear (detection of overall elevation in activity, Supp Fig. 6A). BioAmp and BioBoth trains worked best with biomimetic encoding while BioFreq and Fixed worked best with linear encoding (Supp Fig. 6B). Biomimetic encoding with BioAmp and BioBoth trains resulted in faster detection of onset (mean detection-time(DT)=0.19±0.014s and 0.16±0.011s) than linear encoding with BioFreq and Fixed (DT=0.22±0.019s and 0.20±0.018s). Although this difference was not significant across all trains (p=0.058, Fig. 6C), it was significant when combined within encoding schemes (p=0.019, Fig. 6D). The biomimetic encoding was also much faster at determining offset (DT=0.21±0.016s and 0.19±0.014s) compared to linear encoding (DT=1.42±0.13s and 2.32±0.83s, p<0.001, Fig. 6E). Biomimetic encoding also resulted in less false alarms (FAs, early detection) for onset (FAs=3 and 2) than BioFreq and Fixed (FAs=12 and 21). Using a simple threshold of +3 baseline standard deviations as a cut-off for detection resulted similarly in better performance for BioAmp and BioBoth trains (Supp. Fig. 6C,D,E). The simple threshold method resulted in less FAs (12 and 17 less) for the onset for BioFreq and Fixed than the IDA with increased DTs (0.037±0.012s and 0.041±0.015s more, p<0.05 paired-sample t-test), but resulted in an increase in FAs (12,4,17, and 9 more) for all trains for offset detection (Supp. Fig. 6F,G). For an ideal observer, the strong transients evoked by biomimetic amplitude modulation allows for better classification of the onset and offset of input.

Intensity of ICMS can be used to determine features of sensory input, such as object compliance [11],[22]. Classifiers were additionally trained to discriminate low and high amplitudes (Long vs. Long+). Classifiers were able to discriminate adjusted Long and Long+ fluorescent profiles significantly above chance levels (p<0.01, Fisher's test) for all trains (means=76.9±2.5%, 77.2±3.2%, 82.9±3.2%, and 83.2±3.3%) and these accuracies were not significantly different across trains (p=0.28, Fig. 6F). An ideal observer discriminates ICMS intensity based on the evoked activity with high accuracy for all train types. Overall, biomimetic amplitude modulation improved classification of onset and offset by evoking distinct onset and offset transients, and maintained the ability to discriminate different intensities of ICMS.

Discussion

Biomimetic amplitude, but not frequency, modulation evokes strong onset and offset responses

Biomimetic modulation of ICMS may improve the function and quality of sensory feedback [12],[13]. We wanted to know how biomimetic modulation of ICMS affects cortical neuron recruitment. Most neurons were well modulated by biomimetic amplitude but not frequency (Fig. 2). This agrees with preliminary data in humans, where biomimetic amplitude but not frequency improved perceived naturalness [27]. Here, a small group of neurons were modulated by dynamic frequency changes (Fig. 4C). The presence of these neurons may affect the local response to ICMS frequency, which could explain different evoked percepts of varying discriminability across electrodes in humans [4],[9]. Neurons can have preferential responses to ICMS frequencies related to distance from the electrode [31],[32]. Further studies to understand why different neurons have preferred temporal profiles can shed light on the effects of frequency modulation. Biomimetic amplitude modulation, which

consistently evoked distinct onset and offset transients, should more consistently evoke neural transients similar to those present in recorded neural data [16],[18].

Different ICMS encoding schemes produce fundamentally different responses in individual neurons

Short trains evoked consistent activation of neurons overall. Long trains evoked more response types based on changes in activity over time, which were classified as Rapidly Adapting (RA), Slowly Adapting (SA), or Steady State (SS) (Fig. 4). Identification of RA, SA, and SS trains were significantly correlated across the Fixed and BioFreq trains for the Long and Long+ versions (Supp. Fig. 5). However, there was no correlation of ROI labels for the BioAmp and BioBoth trains with ROI labels for the BioFreq and Fixed trains or labels for the Short with the Long trains. The measured patterns then likely do not reflect simple consistent responses of individual neurons, but reflect more complex emergent processes of the network (as a consequence of connections across diverse populations of neurons). Understanding the response of individual neurons to ICMS then will likely be insufficient to understand the effects of ICMS on perception and a systems level understanding across neural populations will be critical. Future studies should focus on the roles of different neurons and their connections within the network on the response to different stimulus parameters.

Biomimetic amplitude modulation maintains neural excitability over long periods of stimulation

Adaptation is a normal part of sensory processing [28],[49] and may contribute to an increased ability to respond to changes in sensory input. Adaptation of perceived intensity has been observed in peripheral nerve stimulation [50],[51], visual cortex stimulation [52], and somatosensory cortex stimulation [10]. Additionally, stimulation induced depression of neuronal excitability has been observed in multiple animal models [31],[32],[53]–[55]. However, it is not clear how well stimulation evoked adaptation matches normal adaptive processes. Continuous ICMS in somatosensory cortex can lead to complete loss of perception of ICMS within one minute in humans [10]. This could make ICMS ineffective when provided over clinically meaningful time periods. Here, biomimetic amplitude modulation was better able to maintain activation over long periods of time by transiently encoding sensory input, which could allow sensory feedback to be provided for extended periods of time for BCIs.

Mechanisms underlying neural responses to biomimetic ICMS

Adaptation may occur at two time-scales: rapid and slow [28], similar to the phases we observed here (Fig. 5). Rapid and slow adaptation may occur under different mechanisms and may depend on intrinsic properties of different cell types and their synaptic connections and role in larger circuits [29]. One possibility is that rapid adaptation is driven by recruited inhibition and slow adaptation is driven by slower metabolic changes or plasticity. Indeed, inhibitory neurons play an important role in normal adaptation and different inhibitory subtypes can play different and opposing roles in this process [56]–[59]. ICMS can drive sparse and distributed activation of excitatory neurons by recruiting passing axons [33],[60],[61] but the recruitment of inhibitory neurons near the electrode may contribute to more focal activation of functional units for feature encoding after onset [62]–[65]. Here, higher amplitudes and frequencies drove more rapid adaptation of neurons, agreeing with previous results [31],[32],[36],[66]. Higher frequencies and amplitudes then may result in increased recruitment of inhibitory neurons [35] at onset, driving strong rapid adaptation. RA neurons were significantly farther from the electrode than SS neurons. SS neurons likely represent neurons directly recruited by ICMS while distant RA neurons are synaptically recruited [67]. Electrical stimulation can drive continuous activation of directly-recruited neurons despite inhibitory drive, while those recruited synaptically are likely adapted. However, because the cortex normally responds transiently to sensory input, this consistent inhibitory drive may reflect unnatural pressures on synaptically recruited neurons. By reducing the amplitude during the hold phase, biomimetic amplitude modulation better maintains excitability of neurons farther from the electrode, which may better reflect normal cortical activation and allow for stronger encoding of changes in stimulus input.

		Onset			Hold			Offset				
		% ROIs	Intensity	Distance	% ROIs	Intensity	Distance	% ROIs	Intensity	Distance	Adaptation within train	Adaptation across trials
Bio Amp	**Short**	++++	++++	+++	N/A	N/A	N/A	N/A	N/A	N/A	+	+
	Long	++++	++	++++	+	++	++++	++++	+++	++++	+	++
	Long+	++++	+	++++	+	+	+	++++	++++	++++	+	+
Bio Both	**Short**	+++	+	++++	N/A	N/A	N/A	N/A	N/A	N/A	++	+++
	Long	+++	+	+++	++	+	+	+++	++++	+++	++	+
	Long+	++	++	+++	++	+++	+++	+++	+++	+++	++	++
Bio Freq	**Short**	++	+++	++	N/A	N/A	N/A	N/A	N/A	N/A	+++	++++
	Long	++	++++	+	++++	+++	+++	++	+	++	++++	++++
	Long+	+++	++++	++	++++	++++	++++	++	++	++	+++	++++
Fix	**Short**	+	++	+	N/A	N/A	N/A	N/A	N/A	N/A	++++	++
	Long	+	+++	++	+++	++++	++	+	++	+	+++	+++
	Long+	+	+++	+	+++	++	++	+	+	+	++++	+++

Table 2: Summary table of mean effects of each train type in comparison to one another. BioAmp trains evoked activation in more ROIs during onset and offset, while BioFreq trains evoked activation in the most ROIs during the hold phase. BioAmp trains recruited the farthest neurons and drove the least adaptation both within and across trials. The plus marks indicate the mean magnitude of each measure, where ++++ have the highest magnitude and + have the least magnitude. Short trains were too short to divide into multiple phases, so all outcomes were grouped into the onset phase (and other phases are marked with "N/A"). Colors were used to indicate desirable outcomes: it was assumed that greater neural recruitment with less charge injection and less adaptation are both desirable. Dark yellow represents the best clinical effect while light-yellow/white indicates the worst clinical effect. Under these assumptions, BioAmp trains have the greatest assumed desirable effects as indicated by the preponderance of dark yellow labels.

Conclusion: Implications for brain-computer interfaces

ICMS is an emerging approach to restore sensations, primarily somatosensory and visual. Traditionally, researchers have encoded sensory input directly with linear/engineered approaches. Here, biomimetic amplitude modulation evoked strong onset and offset responses. It has been found previously that the initial confidence in sensory input is critical for improved robotic arm control with sensory feedback [11]. We also found that all trains resulted in high success in intensity discrimination for an ideal observer, which agree with object identification results in humans [22]. Biomimetic amplitude modulation also maintained excitability over long periods of stimulation and reduced the total charge injection. Because continuous stimulation, especially at high amplitudes or frequencies, can lead to electrode degradation [68],[69], reducing charge injection may improve the longevity of implanted arrays. Under the assumptions that higher activation with lower charge injection and less adaptation are desirable, biomimetic amplitude modulation are better than traditional engineered approaches (Table 2). This simple modification to ICMS encoding then may provide many benefits for clinical applications.

Acknowledgements: The authors would like to thank Kevin Stieger, Keying Chen, Naofumi Suematsu, Fan Li, and Adam Forrest for feedback. This work was supported by NIH T32 NS086749, R01NS105691, R01NS115707 and NSF CAREER CBET 1943906.

References

[1] S. N. Flesher *et al.*, "Intracortical microstimulation of human somatosensory cortex," *Sci Transl Med*, vol. 8, no. 361, pp. 1–11, 2016, doi: 10.1126/scitranslmed.aaf8083.

[2] M. Armenta Salas *et al.*, "Proprioceptive and cutaneous sensations in humans elicited by intracortical microstimulation," *Elife*, no. 7, p. e32904, 2018, doi: 10.7554/eLife.32904.

[3] M. S. Fifer *et al.*, "Intracortical Somatosensory Stimulation to Elicit Fingertip Sensations in an Individual with Spinal Cord Injury," *Neurology*, vol. 98, no. 7, pp. E679–E687, 2022, doi: 10.1212/WNL.0000000000013173.

[4] C. L. Hughes, S. N. Flesher, J. M. Weiss, M. L. Boninger, J. Collinger, and R. Gaunt, "Perception of microstimulation frequency in human somatosensory cortex," *Elife*, vol. 10, Jul. 2021, doi: 10.7554/ELIFE.65128.

[5] E. Fernández *et al.*, "Visual percepts evoked with an Intracortical 96-channel Microelectrode Array inserted in human occipital cortex," *J Clin Invest*, 2021, Accessed: Oct. 22, 2021. [Online]. Available: https://www.jci.org/articles/view/151331

[6] R. Romo, A. Hernández, A. Zainos, and E. Salinas, “Somatosensory discrimination based on cortical microstimulation,” *Nature*, vol. 392, no. 6674, pp. 387–390, 1998, doi: 10.1038/32891.

[7] R. Romo, A. Hernández, A. Zainos, C. D. C. D. Brody, and L. Lemus, “Sensing without touching: psychophysical performance based on cortical microstimulation.,” *Neuron*, vol. 26, no. 1, pp. 273–8, Apr. 2000, doi: 10.1016/S0896-6273(00)81156-3.

[8] T. Callier, N. W. Brantly, A. Caravelli, and S. J. Bensmaia, “The frequency of cortical microstimulation shapes artificial touch,” *Proc Natl Acad Sci U S A*, vol. 117, no. 2, pp. 1191–1200, 2020, doi: 10.1073/pnas.1916453117.

[9] C. L. Hughes and R. A. Gaunt, “Changes in interpulse spacing changes tactile perception of microstimulation in human somatosensory cortex,” in *10th International IEEE EMBS Conference on Neural Engineering*, 2021, pp. 1–4. Accessed: Jun. 09, 2021. [Online]. Available: https://ieeexplore.ieee.org/abstract/document/9441292/?casa_token=AR1101YucrEAAAAA:ACnR0lQDK7utH6RvVD-OZFoRkU50qpgvM5QPkRAEBb-ZOCx7IhYayKlV9wX16VeuuDhIU-hI3w

[10] C. Hughes, S. Flesher, and R. Gaunt, “Effects of stimulus pulse rate on somatosensory adaptation in the human cortex,” *Brain Stimul*, 2022, Accessed: Aug. 23, 2022. [Online]. Available: https://www.sciencedirect.com/science/article/pii/S1935861X22001000

[11] S. N. Flesher *et al.*, “A brain-computer interface that evokes tactile sensations improves robotic arm control,” 2021.

[12] H. P. Saal and S. J. Bensmaia, “Biomimetic approaches to bionic touch through a peripheral nerve interface,” *Neuropsychologia*, vol. 79, pp. 344–353, 2015, doi: 10.1016/j.neuropsychologia.2015.06.010.

[13] E. v. Okorokova, Q. He, and S. J. Bensmaia, “Biomimetic encoding model for restoring touch in bionic hands through a nerve interface,” *J Neural Eng*, vol. 15, no. 6, 2018, doi: 10.1088/1741-2552/aae398.

[14] K. Kumaravelu *et al.*, “A comprehensive model-based framework for optimal design of biomimetic patterns of electrical stimulation for prosthetic sensation,” *J Neural Eng*, vol. 17, no. 4, Aug. 2020, doi: 10.1088/1741-2552/ABACD8.

[15] E. Formento, E. D’Anna, S. Gribi, S. P. Lacour, and S. Micera, “A biomimetic electrical stimulation strategy to induce asynchronous stochastic neural activity,” *J Neural Eng*, vol. 17, no. 4, p. 046019, Jul. 2020, doi: 10.1088/1741-2552/ABA4FC.

[16] T. Callier, A. K. Suresh, and S. J. Bensmaia, “Neural Coding of Contact Events in Somatosensory Cortex,” *Cerebral Cortex*, 2018, doi: 10.1093/cercor/bhy337.

[17] J. E. Cooke, J. J. Lee, E. L. Bartlett, X. Wang, and D. Bendor, “post-stimulatory activity in primate auditory cortex evoked by sensory stimulation during passive listening,” vol. 10, p. 13885, 2020, doi: 10.1038/s41598-020-70397-0.

[18] S. B. Ryu, P. Werginz, and S. I. Fried, “Response of mouse visual cortical neurons to electric stimulation of the retina,” *Front Neurosci*, vol. 13, no. APR, p. 324, 2019, doi: 10.3389/FNINS.2019.00324/BIBTEX.

[19] H. P. Saal, B. P. Delhaye, B. C. Rayhaun, and S. J. Bensmaia, “Simulating tactile signals from the whole hand with millisecond precision,” *Proc Natl Acad Sci U S A*, vol. 114, no. 28, pp. E5693–E5702, Jul. 2017, doi: 10.1073/pnas.1704856114.

[20] G. Valle *et al.*, “Biomimetic Intraneural Sensory Feedback Enhances Sensation Naturalness, Tactile Sensitivity, and Manual Dexterity in a Bidirectional Prosthesis,” *Neuron*, vol. 100, no. 1, pp. 37–45, 2018, doi: 10.1016/j.neuron.2018.08.033.

[21] J. A. George *et al.*, “Biomimetic sensory feedback through peripheral nerve stimulation improves dexterous use of a bionic hand,” *Sci Robot*, vol. 4, no. 32, 2019, doi: 10.1126/scirobotics.aax2352.

[22] L. E. Osborn *et al.*, “Intracortical microstimulation of somatosensory cortex enables object identification through perceived sensations,” in *2021 43rd Annual International Conference of the IEEE Engineering in Medicine & Biology Society (EMBC)*, Nov. 2021, pp. 6259–6262. doi: 10.1109/EMBC46164.2021.9630450.

[23] N. D. Shelchkova *et al.*, “Microstimulation of human somatosensory cortex evokes task-dependent, spatially patterned responses in motor cortex,” *bioRxiv*, p. 2022.08.10.503543, Oct. 2022, doi: 10.1101/2022.08.10.503543.

[24] C. L. Hughes, A. Herrera, R. Gaunt, and J. Collinger, “Bidirectional brain-computer interfaces,” *Handb Clin Neurol*, vol. 168, pp. 163–181, 2020, Accessed: Mar. 19, 2020. [Online]. Available: https://www.sciencedirect.com/science/article/pii/B9780444639349000135

[25] M. Gerges, E. L. Foldes, D. M. Ackermann, N. Bhadra, N. Bhadra, and K. L. Kilgore, “Frequency and amplitude transitioned waveforms mitigate the onset response in high frequency nerve block,” *J Neural Eng*, vol. 7, no. 6, p. 066003, Dec. 2010, doi: 10.1088/1741-2560/7/6/066003.

[26] Z. Cai, Z. Feng, Z. Guo, W. Zhou, Z. Wang, and X. Wei, “Novel stimulation paradigms with temporally-varying parameters to reduce synchronous activity at the onset of high frequency stimulation in rat hippocampus,” *Front Neurosci*, vol. 11, no. OCT, p. 563, Oct. 2017, doi: 10.3389/FNINS.2017.00563/BIBTEX.

[27] C. Hughes, “Biomimetic Intracortical Microstimulation of Human Somatosensory Cortex for a Bidirectional Brain-computer Interface,” *University of Pittsburgh*, 2021, Accessed: Apr. 19, 2022. [Online]. Available: http://d-scholarship.pitt.edu/41432/

[28] B. Wark, B. N. Lundstrom, and A. Fairhall, “Sensory adaptation,” *Current Opinion in Neurobiology*, vol. 17, no. 4. pp. 423–429, 2007. doi: 10.1016/j.conb.2007.07.001.

[29] C. J. Whitmire and G. B. Stanley, “Rapid Sensory Adaptation Redux: A Circuit Perspective,” *Neuron*, vol. 92, no. 2. pp. 298–315, 2016. doi: 10.1016/j.neuron.2016.09.046.

[30] K. C. Stieger, J. R. Eles, K. A. Ludwig, and T. D. Y. Kozai, “In vivo microstimulation with cathodic and anodic asymmetric waveforms modulates spatiotemporal calcium dynamics in cortical neuropil and pyramidal neurons of male mice,” *J Neurosci Res*, vol. 98, no. 10, pp. 2072–2095, Oct. 2020, doi: 10.1002/jnr.24676.

[31] N. J. Michelson, J. R. Eles, A. L. Vazquez, K. A. Ludwig, and T. D. Y. Kozai, “Calcium activation of cortical neurons by continuous electrical stimulation: Frequency dependence, temporal fidelity, and activation density,” *J Neurosci Res*, vol. 97, no. 5, pp. 620–638, May 2019, doi: 10.1002/jnr.24370.

[32] J. R. Eles, K. C. Stieger, and T. D. Y. Kozai, “The temporal pattern of intracortical microstimulation pulses elicits distinct temporal and spatial recruitment of cortical neuropil and neurons,” *J Neural Eng*, vol. 18, no. 1, p. 15001, 2021, doi: 10.1088/1741-2552/abc29c.

[33] M. H. Histed, V. Bonin, and R. C. Reid, “Direct Activation of Sparse, Distributed Populations of Cortical Neurons by Electrical Microstimulation,” *Neuron*, vol. 63, no. 4, pp. 508–522, Aug. 2009, doi: 10.1016/j.neuron.2009.07.016.

[34] M. H. Histed, A. M. Ni, and J. H. R. Maunsell, “Insights into cortical mechanisms of behavior from microstimulation experiments,” *Prog Neurobiol*, vol. 103, pp. 115–130, Apr. 2013, doi: 10.1016/J.PNEUROBIO.2012.01.006.

[35] M. C. Dadarlat, Y. J. Sun, and M. P. Stryker, “Spatiotemporal recruitment of inhibition and excitation in the mammalian cortex during electrical stimulation,” *bioRxiv*, p. 2022.06.03.494729, Jun. 2022, doi: 10.1101/2022.06.03.494729.

[36] K. C. Stieger, J. R. Eles, K. A. Ludwig, and T. D. Y. Kozai, “Intracortical microstimulation pulse waveform and frequency recruits distinct spatiotemporal patterns of cortical neuron and neuropil activation,” *J Neural Eng*, vol. 19, no. 2, p. 026024, Mar. 2022, doi: 10.1088/1741-2552/AC5BF5.

[37] S. Eick *et al.*, “Iridium oxide microelectrode arrays for in vitro stimulation of individual rat neurons from dissociated cultures,” *Front Neuroeng*, vol. 2, no. NOV, Nov. 2009, doi: 10.3389/NEURO.16.016.2009/FULL.

[38] D. McCreery, V. Pikov, and P. R. Troyk, “Neuronal loss due to prolonged controlled-current stimulation with chronically implanted microelectrodes in the cat cerebral cortex.,” *J Neural Eng*, vol. 7, no. 3, p. 036005, Jun. 2010, doi: 10.1088/1741-2560/7/3/036005.

[39] D. B. McCreery, W. F. Agnew, T. G. H. Yuen, and L. Bullara, “Charge density and charge per phase as cofactors in neural injury induced by electrical stimulation,” *IEEE Trans Biomed Eng*, vol. 37, no. 10, pp. 996–1001, 1990, doi: 10.1109/10.102812.

[40] W. Geisler, “Ideal observer analysis,” *The visual neurosciences*, vol. 10, no. 7, pp. 12–12, 2003, Accessed: Jul. 01, 2022. [Online]. Available: http://neurosci.info/courses/vision2/Coding/Geisler_2004.pdf

[41] D. C. Millard and G. B. Stanley, “Anatomically based Bayesian decoding of the cortical response to intracortical microstimulation,” *International IEEE/EMBS Conference on Neural Engineering, NER*, pp. 1457–1460, 2013, doi: 10.1109/NER.2013.6696219.

[42] D. R. Ollerenshaw, H. J. V. Zheng, D. C. Millard, Q. Wang, and G. B. Stanley, “The Adaptive Trade-Off between Detection and Discrimination in Cortical Representations and Behavior,” *Neuron*, vol. 81, no. 5, pp. 1152–1164, Mar. 2014, doi: 10.1016/J.NEURON.2014.01.025.

[43] T. T. R. F. J. Hastie, *The elements of statistical learning: data mining, inference, and prediction*, Vol. 2. New York: Springer, 2009.

[44] Holger Hoffman, “Violin Plot .” MATLAB Central File Exchange, 2022.

[45] David Long, “ellipse.m.” MATLAB Central File Exchange, 2022.

[46] N. G. Kunigk, M. E. Urdaneta, I. G. Malone, F. Delgado, and K. J. Otto, “Reducing Behavioral Detection Thresholds per Electrode via Synchronous, Spatially-Dependent Intracortical Microstimulation,” *Front Neurosci*, vol. 16, Jun. 2022, doi: 10.3389/FNINS.2022.876142.

[47] M. E. Urdaneta, N. G. Kunigk, F. Delgado, S. I. Fried, and K. J. Otto, “Layer-specific parameters of intracortical microstimulation of the somatosensory cortex,” *J Neural Eng*, vol. 18, no. 5, p. 55007, 2021, doi: 10.1088/1741-2552/abedde.

[48] S. Kim, T. Callier, G. a Tabot, R. A. Gaunt, F. v Tenore, and S. J. Bensmaia, “Behavioral assessment of sensitivity to intracortical microstimulation of primate somatosensory cortex,” *Proceedings of the National Academy of Sciences*, vol. 112, no. 49, pp. 15202–15207, Dec. 2015, doi: 10.1073/pnas.1509265112.

[49] S. O’Mara, M. J. Rowe, and R. P. C. Tarvin, “Neural mechanisms in vibrotactile adaptation,” *J Neurophysiol*, vol. 59, no. 2, pp. 607–622, 1988, doi: 10.1152/JN.1988.59.2.607.

[50] E. L. Graczyk, B. P. Delhaye, M. A. Schiefer, S. J. Bensmaia, and D. J. Tyler, “Sensory adaptation to electrical stimulation of the somatosensory nerves,” *J Neural Eng*, vol. 15, no. 4, p. 046002, May 2018, doi: 10.1088/1741-2552/aab790.

[51] G. Valle *et al.*, “Comparison of linear frequency and amplitude modulation for intraneural sensory feedback in bidirectional hand prostheses,” *Sci Rep*, vol. 8, no. 1, pp. 1–13, 2018, doi: 10.1038/s41598-018-34910-w.

[52] E. M. Schmidt, M. J. Bak, F. T. Hambrecht, C. v. Kufta, D. K. O'Rourke, and P. Vallabhanath, "Feasibility of a visual prosthesis for the blind based on intracortical micro stimulation of the visual cortex," *Brain*, vol. 119, no. 2, pp. 507–522, Apr. 1996, doi: 10.1093/brain/119.2.507.

[53] A. Ray, E. J. Lee, M. S. Humayun, and J. D. Weiland, "Continuous electrical stimulation decreases retinal excitability but does not alter retinal morphology," *J Neural Eng*, vol. 8, no. 4, p. 045003, Jul. 2011, doi: 10.1088/1741-2560/8/4/045003.

[54] D. B. McCreery, W. F. Agnew, and L. A. Bullara, "The Effects of Prolonged Intracortical Microstimulation on the Excitability of Pyramidal Tract Neurons in the Cat," *Annals of Biomedical Engineering 2002 30:1*, vol. 30, no. 1, pp. 107–119, 2002, doi: 10.1114/1.1430748.

[55] D. B. McCreery, T. G. H. Yuen, W. F. Agnew, and L. A. Bullara, "A characterization of the effects on neuronal excitability due to prolonged microstimulation with chronically implanted microelectrodes," *IEEE Trans Biomed Eng*, vol. 44, no. 10, pp. 931–939, Oct. 1997, doi: 10.1109/10.634645.

[56] L. J. Baruchin, F. Ghezzi, M. M. Kohl, and S. J. B. Butt, "Contribution of Interneuron Subtype-Specific GABAergic Signaling to Emergent Sensory Processing in Mouse Somatosensory Whisker Barrel Cortex," *Cerebral Cortex*, vol. 32, no. 12, pp. 2538–2554, Jun. 2022, doi: 10.1093/CERCOR/BHAB363.

[57] L. L. Glickfeld, M. H. Histed, and J. H. R. Maunsell, "Mouse Primary Visual Cortex Is Used to Detect Both Orientation and Contrast Changes," *Journal of Neuroscience*, vol. 33, no. 50, pp. 19416–19422, Dec. 2013, doi: 10.1523/JNEUROSCI.3560-13.2013.

[58] R. G. Natan, W. Rao, and M. N. Geffen, "Cortical Interneurons Differentially Shape Frequency Tuning following Adaptation," *Cell Rep*, vol. 21, no. 4, pp. 878–890, 2017, doi: 10.1016/j.celrep.2017.10.012.

[59] R. G. Natan *et al.*, "Complementary control of sensory adaptation by two types of cortical interneurons," *Elife*, vol. 4, no. OCTOBER2015, 2015, doi: 10.7554/eLife.09868.

[60] C. K. Overstreet, J. D. Klein, and S. I. Helms Tillery, "Computational modeling of direct neuronal recruitment during intracortical microstimulation in somatosensory cortex," *J Neural Eng*, vol. 10, no. 6, p. 066016, Dec. 2013, doi: 10.1088/1741-2560/10/6/066016.

[61] K. Kumaravelu, J. Sombeck, L. E. Miller, S. J. Bensmaia, and W. M. Grill, "Stoney vs. Histed: Quantifying the spatial effects of intracortical microstimulation," *Brain Stimul*, vol. 15, no. 1, pp. 141–151, Jan. 2022, doi: 10.1016/J.BRS.2021.11.015.

[62] M. Osanai, S. Tanaka, Y. Takeno, S. Takimoto, and T. Yagi, "Spatiotemporal Properties of the Action Potential Propagation in the Mouse Visual Cortical Slice Analyzed by Calcium Imaging," *PLoS One*, vol. 5, no. 10, p. e13738, 2010, doi: 10.1371/JOURNAL.PONE.0013738.

[63] Y. Tanaka *et al.*, "Focal activation of neuronal circuits induced by microstimulation in the visual cortex," *J Neural Eng*, vol. 16, no. 3, p. 036007, Mar. 2019, doi: 10.1088/1741-2552/AB0B80.

[64] A. Hayashi, T. Yoshida, and K. Ohki, "Cell type specific representation of vibro-tactile stimuli in the mouse primary somatosensory cortex," *Front Neural Circuits*, vol. 12, Dec. 2018, doi: 10.3389/FNCIR.2018.00109/FULL.

[65] M. Prsa, K. Morandell, G. Cuenu, and D. Huber, "Feature-selective encoding of substrate vibrations in the forelimb somatosensory cortex," *Nature*, 2019, doi: 10.1038/s41586-019-1015-8.

[66] Z. Feng, X. Zheng, Y. Yu, and D. M. Durand, "Functional disconnection of axonal fibers generated by high frequency stimulation in the hippocampal CA1 region in-vivo," *Brain Res*, vol. 1509, pp. 32–42, May 2013, doi: 10.1016/J.BRAINRES.2013.02.048.

[67] J. T. Sombeck *et al.*, "Characterizing the short-latency evoked response to intracortical microstimulation across a multi-electrode array," *J Neural Eng*, vol. 19, no. 2, p. 026044, Apr. 2022, doi: 10.1088/1741-2552/AC63E8.

[68] S. Negi, R. Bhandari, L. Rieth, R. van Wagenen, and F. Solzbacher, “Neural electrode degradation from continuous electrical stimulation: Comparison of sputtered and activated iridium oxide,” *J Neurosci Methods*, vol. 186, no. 1, pp. 8–17, Jan. 2010, doi: 10.1016/j.jneumeth.2009.10.016.

[69] K. Woeppel *et al.*, “Explant Analysis of Utah Electrode Arrays Implanted in Human Cortex for Brain-Computer-Interfaces,” *Front Bioeng Biotechnol*, vol. 9, p. 1137, Dec. 2021, doi: 10.3389/FBIOE.2021.759711/BIBTEX.

	Short trains	Long trains	Long trains+	Cortical area	Sex
Mouse 1	2	0	0	Visual cortex	Male
Mouse 2	2	0	0	Visual cortex	Female
Mouse 3	2	0	0	Visual cortex	Female
Mouse 4	2	2	0	Visual cortex	Male
Mouse 5	2	2	0	Visual cortex	Female
Mouse 6	1	1	1	Visual cortex	Female
Mouse 7	1	1	1	Somatosensory cortex	Male
Mouse 8	1	1	1	Somatosensory cortex	Male
Mouse 9	1	1	1	Somatosensory cortex	Female
Mouse 10	1	1	1	Visual cortex	Male
Mouse 11	1	1	1	Somatosensory cortex	Female
Mouse 12	1	1	1	Visual cortex	Male

Supplementary Table 1: **Mice used for all experiments and corresponding trains presented/area stimulated.** Mice are named based on the chronological order in which the animals were tested. Short trains represent the 1-s on 4-s off paradigm. Long trains represent the 30-s on 15-s off paradigm. Long trains+ represent the 30-s on 15-s off paradigm at an elevated amplitude.

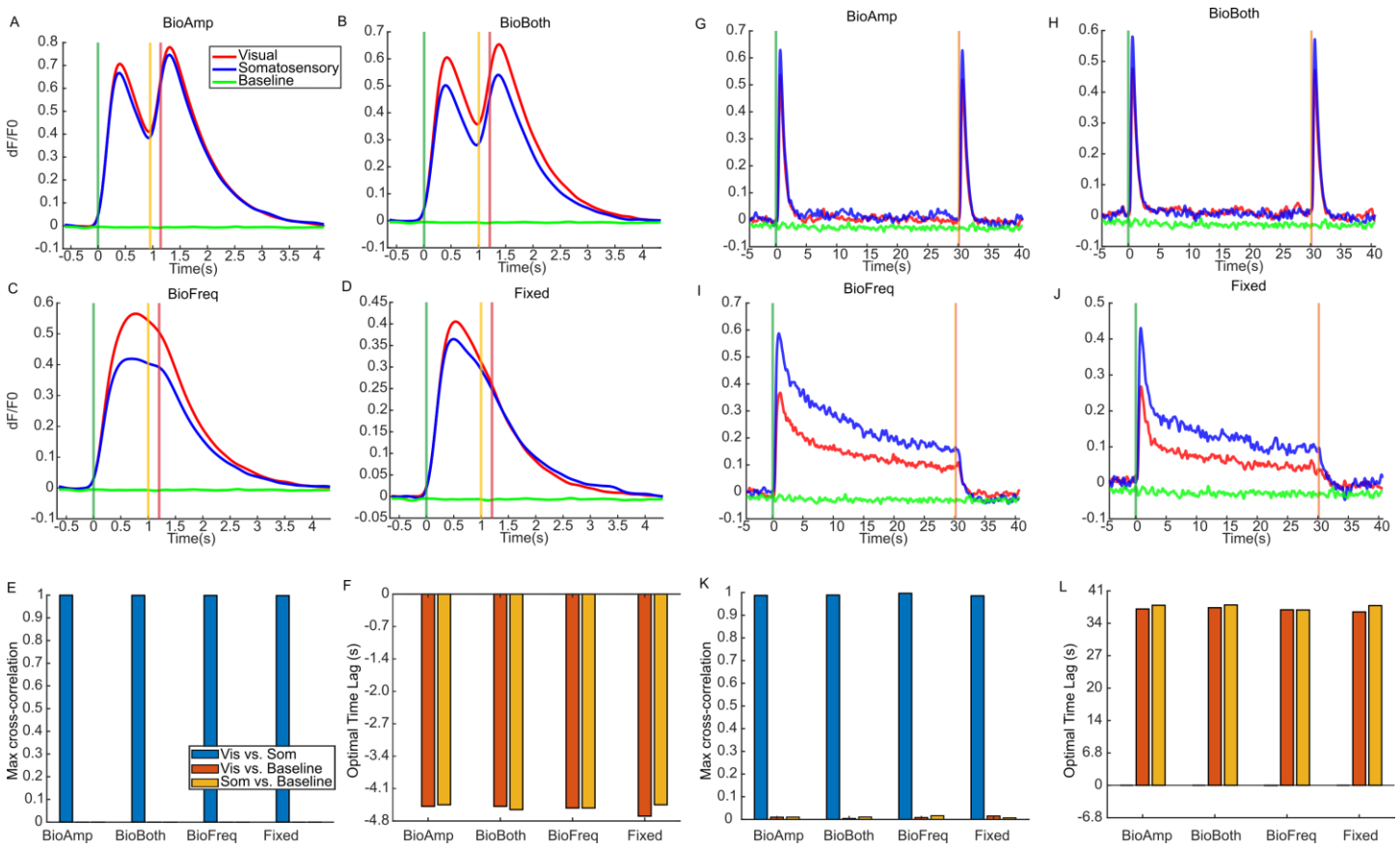

Supplementary Figure 1: Responses are similar across somatosensory and visual cortices. A-D) Average traces for Short trains plotted for visual cortex (*n*=8), somatosensory cortex (*n*=4), and baseline (no ICMS, *n*=10). E) The max correlation value for cross-correlation between somatosensory and visual cortex, visual cortex and baseline, and somatosensory cortex and baseline for Short trains. The correlation value of near 1 shows a strong correlation between the evoked responses between visual and somatosensory cortex. F) The optimal lag for cross-correlations for Short trains (the lag between time series that maximizes the correlation). The value near 0 shows a strong temporal overlap in the evoked responses between visual and somatosensory cortex. G-J) Average traces for Long trains plotted for visual cortex (*n*=5), somatosensory cortex (*n*=4), and baseline (no ICMS, *n*=7). K) The max correlation value for cross-correlation for Long trains. L) The optimal lag for cross-correlations for Long trains.

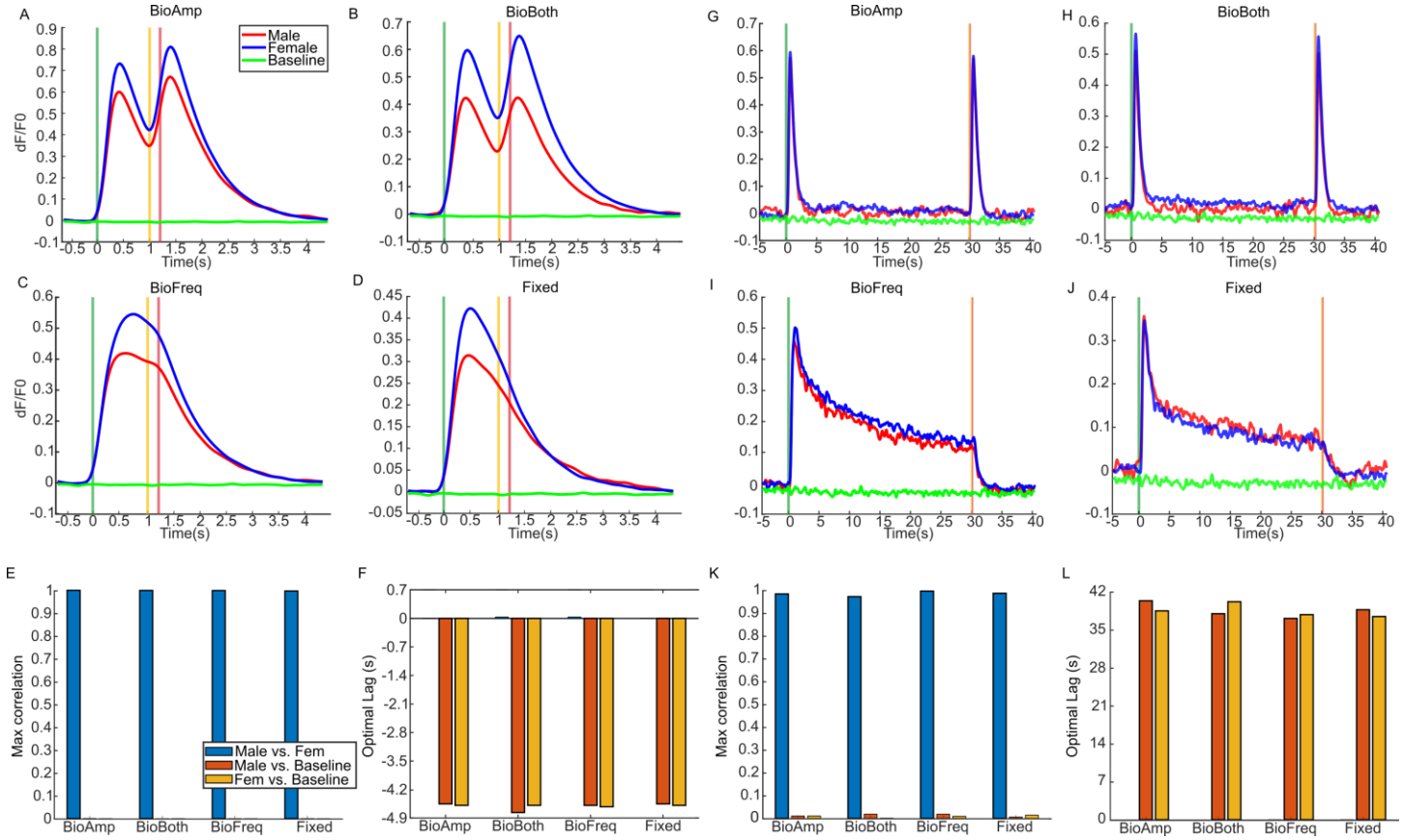

Supplementary Figure 2: Responses are similar across animal sex. A-D) Average traces for Short trains plotted for males (*n*=6), females (*n*=6), and baseline (no ICMS, *n*=10). E) The max correlation value for cross-correlation between males and females, males and baseline, and females and baseline for Short trains. <u>The correlation value of near 1 shows a strong correlation between the evoked responses between visual and somatosensory cortex.</u> F) The optimal lag for cross-correlations for Short trains (the lag between time series that maximizes the correlation). <u>The value near 0 shows a strong temporal overlap in the evoked responses between visual and somatosensory cortex</u> G-J) Average traces for Long trains plotted for males (*n*=5), females (*n*=4), and baseline (no ICMS, *n*=7). K) The max correlation value for cross-correlation for Long trains. L) The optimal lag for cross-correlations for Long trains.

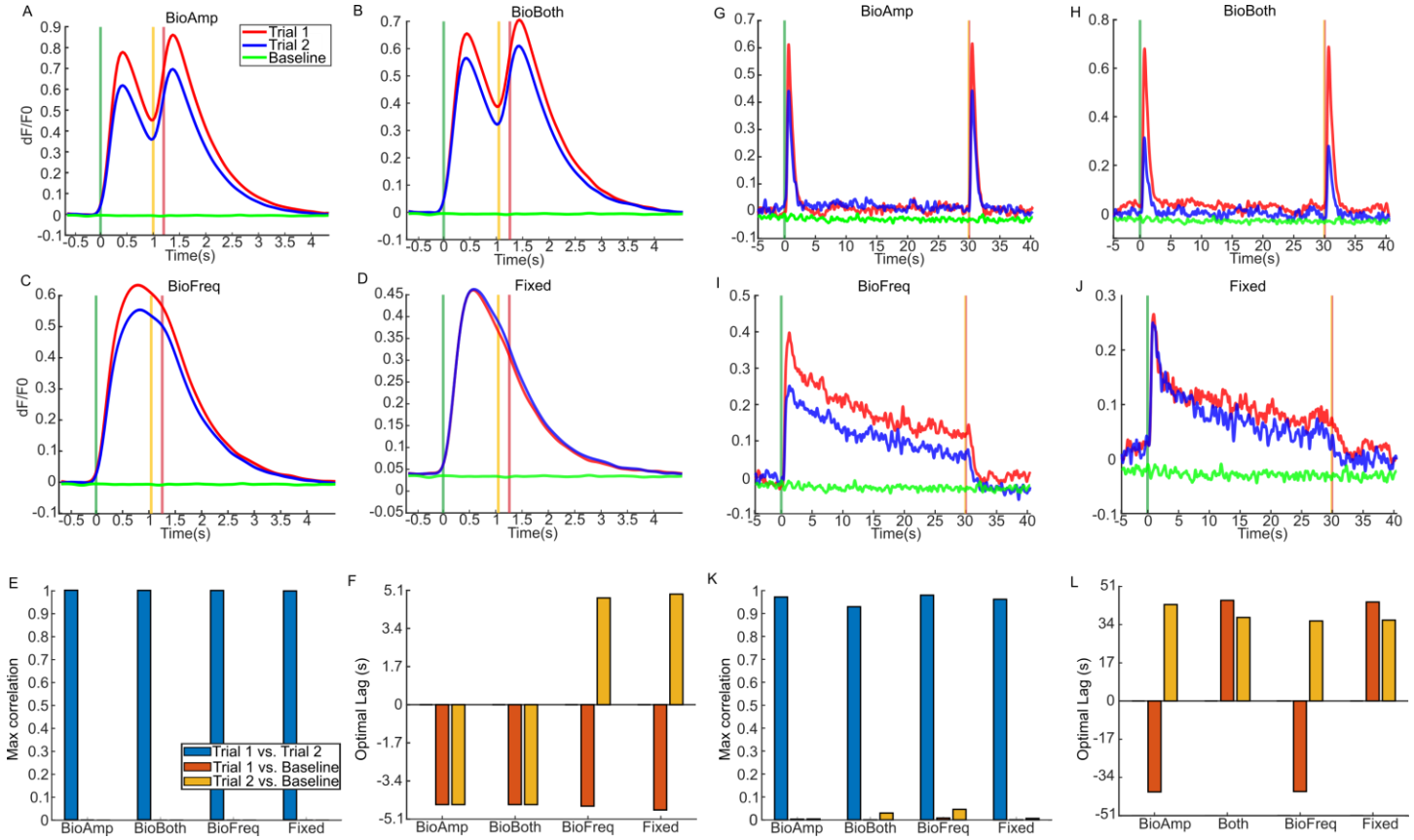

Supplementary Figure 3: Responses are similar across trials. A-D) Average traces for Short trains plotted for trial 1 (*n*=5), trial 2 (*n*=5), and baseline (no ICMS, *n*=10). E) The max correlation value for cross-correlation between trial 1 and trial 2, trial 1 and baseline, and trial 2 and baseline for Short trains. The correlation value of near 1 shows a strong correlation between the evoked responses between visual and somatosensory cortex. F) The optimal lag for cross-correlations for Short trains (the lag between time series that maximizes the correlation). The value near 0 shows a strong temporal overlap in the evoked responses between visual and somatosensory cortex G-J) Average traces for Long trains plotted for trial 1 (*n*=2), trial 2 (*n*=2), and baseline (no ICMS, *n*=7). K) The max correlation value for cross-correlation for Long trains. L) The optimal lag for cross-correlations for Long trains.

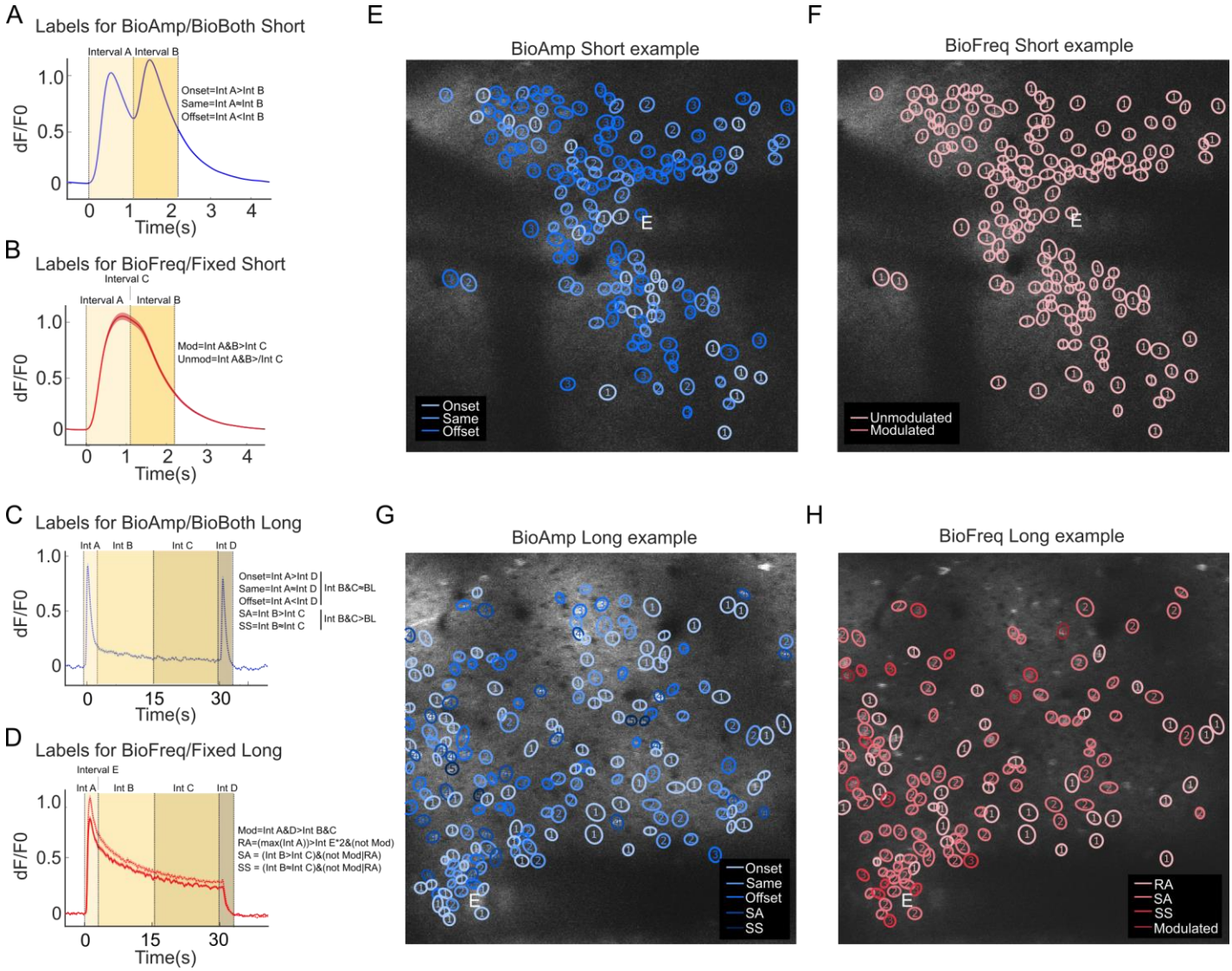

Supplementary Figure 4: Neurons were divided based on identified spatiotemporal characteristics. A) Short BioAmp and BioBoth trains were identified to have differences in the location of maximum peak. If the first peak was greater than the second peak by at least 0.5x standard deviations of the noise, then the ROI was identified as "Onset." If the second peak was greater, the ROI was identified as "Offset." If the peaks were not different by more than 0.5x standard deviations of the noise, then the ROI was identified as "Same." B) Short BioFreq trains were identified to have a small number of ROIs that were modulated by the onset and offset transients. These "Modulated" ROIs were separated if they had maximum intensities during the Onset and Offset period that was greater than the Hold period by more than 0.5x standard deviations of the noise. ROIs that did not have this difference were labeled "Unmodulated." All Fixed trains were identified as "Unmodulated." C) Long and Long+ BioAmp and BioBoth trains were identified similarly with "Onset," "Same," and "Offset," but additionally had some ROIs that had elevated activity during the hold period, which were separated as "Slowly Adapting" (SA) or "Steady State" (SS). SA ROIs had a maximum intensity in the second half of the hold period that was less than the first half by at least 0.5x standard deviations while SS ROIs had a maximum in the second half that was not different than the first half by at least 0.5x standard deviations. D) Long and Long+ BioFreq and Fixed trains similarly had SA and SS responses, but also had "Rapidly Adapting" (RA) responses. These RA responses were characterized by the maximum intensity at 10-s after stimulation decreasing to less than half of the maximum intensity within the first 10-s. E-H) Examples of active ROIs and their labels for a BioAmp Short (E), BioFreq Short (F), BioAmp Long+ (G) and BioFreq Long+ (H) trains. The white letter E indicates the electrode location. Each circle shows a manually labeled ROI that was exported from ImageJ and fit with an ellipse in MATLAB [45]. Colors and numbers indicate the label classification of each ROI.

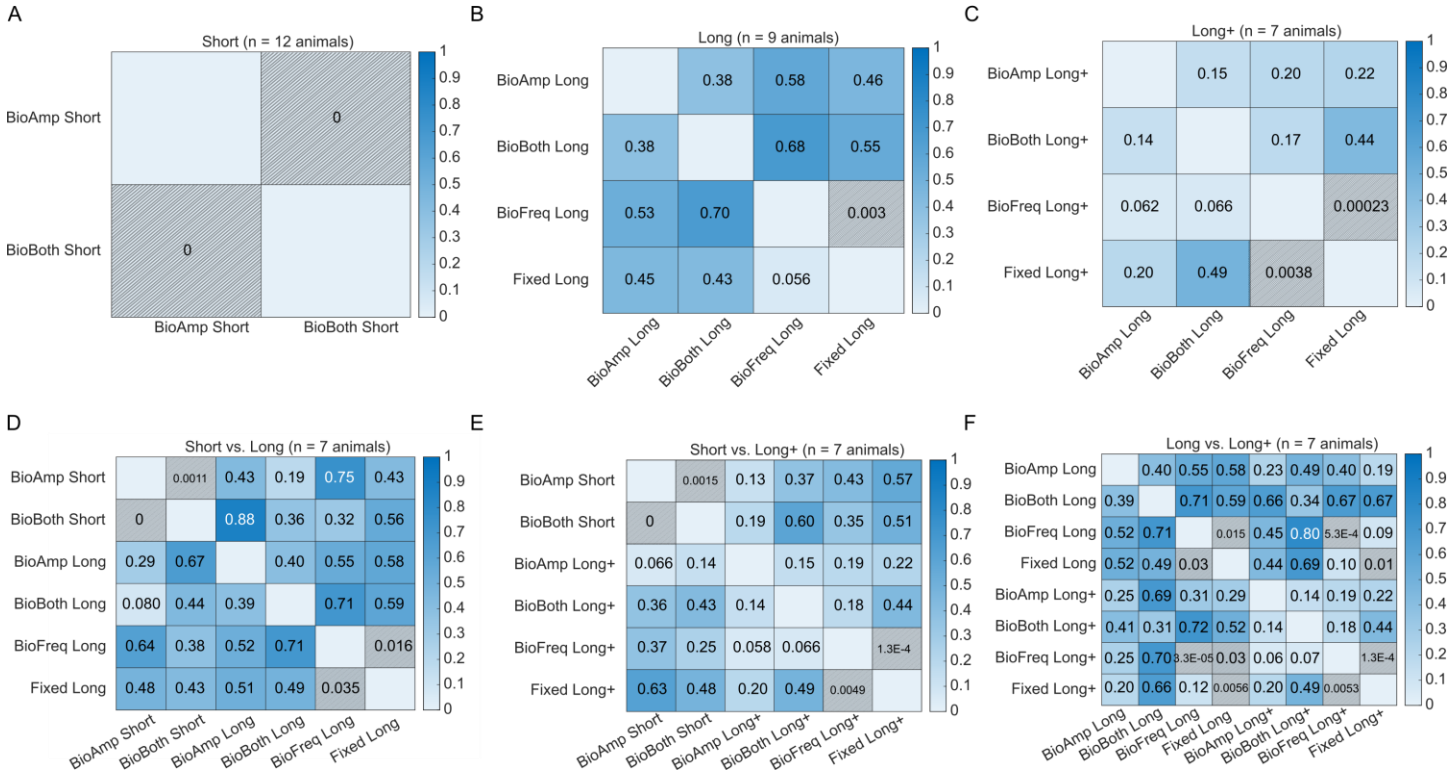

Supplementary Figure 5: Correlation analysis reveals short BioAmp and BioBoth train labels and Long and Long+ BioFreq and Fixed train labels are predictive of each other. Pseudo p-values were calculated for correlation between labels using Equation 2 for each pair of trains, which formed up to a 5x5 matrix. For each train pair, the average p-value of the diagonal was calculated, representing the average significance of correlations between labels. Each of these mean p-vales for each train pair are shown here. Significant p-values are highlighted with gratings. A) Comparison of Short BioAmp and BioBoth train labels. The labels were highly predictive of each other (p=0) indicating that the response to BioAmp Short and BioBoth Short is highly correlated. BioFreq and Fixed are not included here because of the low number of samples of "Modulated" trains for BioFreq trains and the lack of distinct classes for the Fixed trains. B) Comparison of all Long trains. BioFreq and Fixed Long trains are significantly correlated. C) Comparison of all Long+ trains. BioFreq and Fixed Long+ trains are significantly correlated. D) Comparison of Short and Long trains. Short and Long train labels were not predictive of each other. E) Comparison of Short and Long+ trains. Short and Long+ train labels were not predictive of each other. F) Comparison of Long and Long+ trains. BioFreq and Fixed Long and Long+ trains had significant correlations in labels.

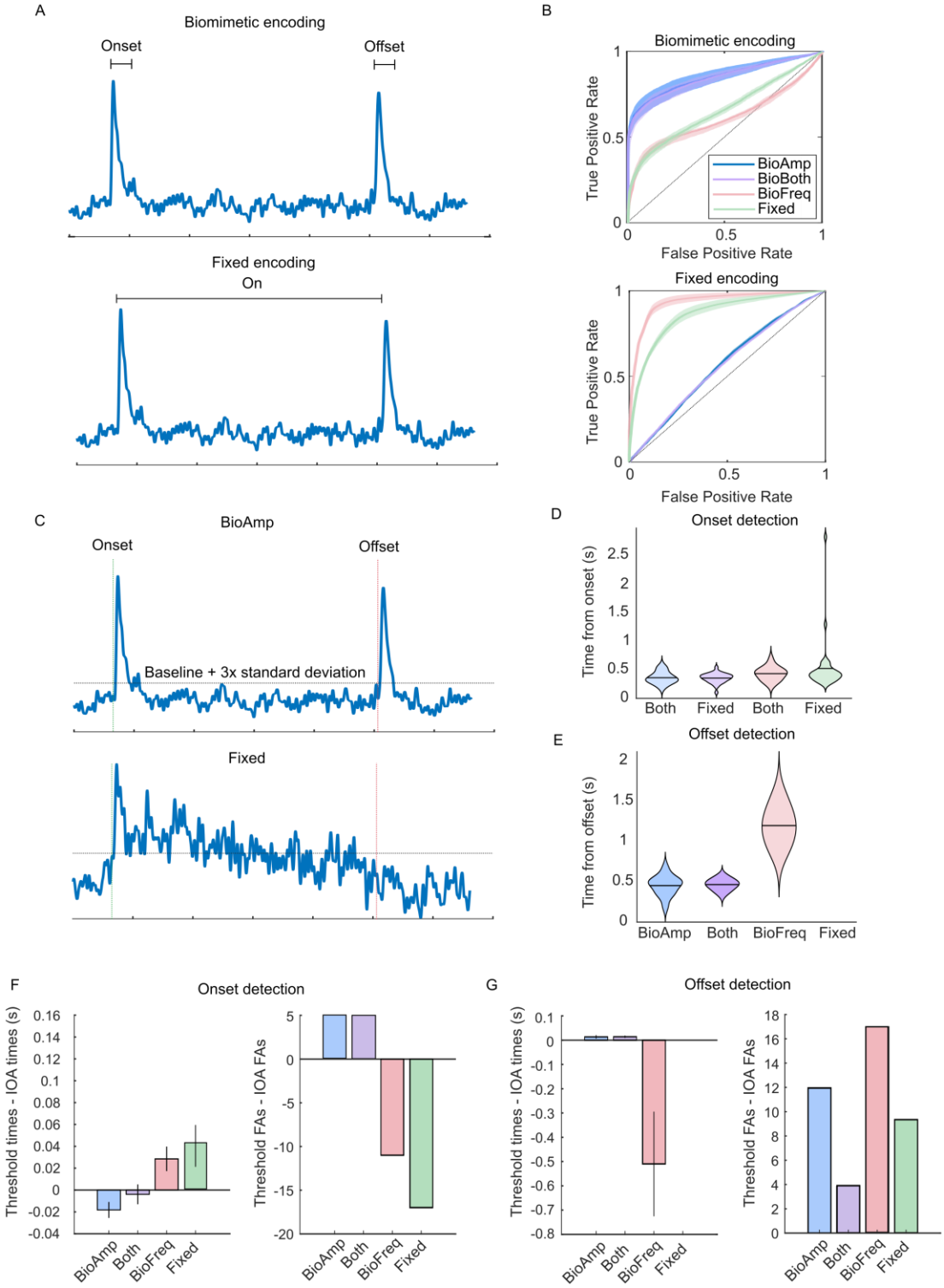

Supplementary Figure 6: Encoding training schemes for ideal observer analysis. A) We used two methods of encoding: biomimetic (top) or fixed (bottom). For biomimetic encoding, onset and offset periods were labeled and input to the classifier. For fixed encoding the total on period (onset and the hold period) were labeled and input to the classifier. Here, those periods are marked on an example BioAmp trace. B) Performance of each classifier for each train type assessed with a Receiver Operator characteristic. The BioAmp and BioBoth trains had a larger area under the curve for the biomimetic encoding scheme, while the Fixed and BioFreq trains had a larger area under the curve for the fixed encoding scheme. C) Using just the Baseline + 3x standard deviation to determine the onset/offset or on period for an example BioAmp (top) and example Fixed (bottom) train. D) Onset detection for each train using the simple baseline+noise threshold. E) Offset detection for each train using the simple baseline+noise threshold. Note that there is no mean for Fixed because all Fixed trains resulted in early detection of offset due to the adapting responses (false alarm). F) Comparison of onset determination with the simple threshold method and ideal observer analysis. Onset detection was slightly faster for BioAmp and BioBoth trains and slower for BioFreq and Fixed trains with IOA. IOA resulted in less false alarms for BioAmp and BioBoth trains but more false alarms for BioFreq and Fixed trains. G) The simple threshold method resulted in lower offset times for BioFreq and similar times for BioAmp and BioFreq. The simple threshold method resulted in much more false alarms for offset across all trains.